AN ACCURATE BEAM MODEL FOR THE NRAO 91 METER RADIO TELESCOPE

by

JAMES ROTHWELL PICHA

B. A. Sc., The University of British Columbia, 1984

A THESIS SUBMITTED IN PARTIAL FULFILLMENT OF
THE REQUIREMENTS FOR THE DEGREE OF
MASTER OF APPLIED SCIENCE

in

THE FACULTY OF GRADUATE STUDIES
DEPARTMENT OF PHYSICS

We accept this thesis as conforming
to the required standard

THE UNIVERSITY OF BRITISH COLUMBIA

September 1986

In presenting this thesis in partial fulfilment of the requirements for an advanced degree at the University of British Columbia, I agree that the Library shall make it freely available for reference and study. I further agree that permission for extensive copying of this thesis for scholarly purposes may be granted by the head of my department or by his or her representatives. It is understood that copying or publication of this thesis for financial gain shall not be allowed without my written permission.

Department of Physics

The University of British Columbia
1956 Main Mall
Vancouver, Canada
V6T 1Y3

Date September 15, 1986

Abstract

Scalar field theory has been used to develop an accurate beam model for use with the National Radio Astronomy Observatory 91 meter radio telescope and the 6 cm dual feed system. The theoretical beam model was calibrated, to an accuracy of 3% of the beam peak, with a small sample of radio point sources within the declination range $23° \leq \delta \leq 62°$. The new beam model is shown to be effective in deconvolving differential beam maps, to a dynamic range of 30:1, by a maximum entropy deconvolution method.

Table of Contents

List of Tables

List of Figures

List of Symbols

a ..... Telescope reflector radius

b ..... Galactic longitude

$B(\theta, \phi)$ ..... Theoretical beam model

$E(\theta, \phi)$ ..... Complex electric field amplitude

$E_{(A)}$ ..... Complex electric field amplitude of feed A

$E_{(B)}$ ..... Complex electric field amplitude of feed B

E_p ..... E plane electric field

E_p^+ ..... E plane electric field (positive y-axis)

E_p^- ..... E plane electric field (negative y-axis)

EX ..... Separation parameter

f ..... Telescope focus

H II ..... Ionized hydrogen nebulae

HPBW ..... Half power beam width

H ..... HPBW of gaussian convolved with the beam model

HAD ..... HPBW of beam A (observed data)

HAM ..... HPBW of beam A (beam model)

HBD ..... HPBW of beam B (observed data)

HBM ..... HPBW of beam B (beam model)

H_p ..... H plane electric field

H_p^+ ..... H plane electric field (positive x-axis)

H_p^- ..... H plane electric field (negative x-axis)

i ..... Complex number

$J_n(\omega)$ ..... Integer order Bessel function

k ..... Wave number

K_s ..... Receiver constant

l ..... Galactic longitude

L ..... Feed leg width

n ..... Number of scans

PRD ..... Peak ratio (observed data)

PRM ..... Peak ratio (beam model)

r ..... Radial integration parameter

$\vec{r}$ ..... Point source vector

$\vec{r_c}$ ..... Beam center vector

$\vec{r_z}$ ..... z-axis vector

R ..... Distance to point source

RT ..... Feed horn rotation angle

SS ..... Separation between peak points (observed data)

SM ..... Separation between peak points (beam model)

t ..... Observation integration time

t_{LF} ..... Equivalent integration time

T_{sys} ..... Receiver system temperature

x ..... Model coordinate x-axis

y ..... Model coordinate y-axis

z ..... Model coordinate z-axis

Z ..... Telescope latitude

* ..... Complex conjugate

α ..... Telescope right ascension

α_c ..... Beam center right ascension

α_z ..... z-axis right ascension

δ ..... Telescope declination

δ_c ..... Beam center declination

δ_z ..... z-axis declination

ΔT_{rms} ..... Receiver noise

Δy ..... y shift parameter

$\Delta \nu_{HF}$ ..... Receiver high frequency bandwidth

$\Delta \phi$ ..... Angle subtended by feed legs

ϵ_x ..... x-axis direction feed horn displacement

ϵ_y ..... y-axis direction feed horn displacement

ϵ_z ..... z-axis direction feed horn displacement

θ ..... Polar angle in model coordinates

θ_c ..... Beam center polar angle in model coordinates

θ' ..... Polar angle integration parameter

λ ..... Wavelength

ϕ ..... Azimuthal angle in model coordinates

ϕ_c ..... Beam center azimuthal angle in model coordinates

ϕ' ..... Azimuthal angle integration parameter

Units

cm ..... centimeters

GHz, MHz, Hz ..... gigaHertz, megaHertz, Hertz

mK, K ..... milliKelvin, Kelvin

^{h} ..... hours of time

$^m, min$ ..... minutes of time

^{s} ..... seconds of time

$^\circ$ ..... degrees

$'$ ..... arcminutes

$''$ ..... arcseconds

Acknowledgements

First I would like to thank my supervisor Dr. P. C. Gregory for his assistance and guidance throughout this work. Also I wish to thank Dr. J. R. Fisher for providing information about the NRAO 91 meter telescope. I am very grateful to M. A. Potts and A. Reid for their advice on computing. Finally, I would like to thank my family for their help in typing and proof reading this manuscript.

I. Introduction

With the Galactic Radio Patrol project, Gregory and Taylor created a unique astronomical data base. In their search for compact source variability, they repeatedly mapped a large portion of the galactic plane ($l = 40°$ to $l = 220°$ and $b = -2°$ to $b = +2°$), using the National Radio Astronomy Observatory (NRAO) 91 meter telescope and a 6 cm dual feed receiver . A full intensity atlas of this region can be created by deconvolving the differential beam pattern from the data, but previous attempts to do this with an empirically derived beam model and a maximum entropy deconvolution method have met with limited success. The major problem seems to have been that the empirical beam model is accurate only to 10% of the beam peak. This work derives a more accurate telescope beam model.

The most direct method of deriving an accurate telescope beam model is to map a large number of point sources spread out over the declination range of the observations. Because the 91 meter telescope is a transit instrument, this mapping requires a large amount of observing time, approximately 21 days for the dual beam system, leaving very little time for the Galactic Radio Patrol observations. To reduce the time spent observing calibration sources, a theoretical telescope beam model has been developed and calibrated with a small number of point sources. It is anticipated that the theoretical beam model will be especially useful for the proposed second phase of the Galactic Radio Patrol project which will use a new seven feed system.

This thesis discusses the theoretical beam used to model the differential beam of the NRAO 91 meter telescope at a wavelength of 6 cm. Specifically the theory used to construct the beam model and the methods used to calibrate the beam model with a small number of point sources are presented in sections II and V. In section VI, the theoretical beam model is compared to the old empirical beam model developed by Taylor (1982) and Braun (1981),and the maximum entropy deconvolution method is used to do

dynamic range tests of the theoretical beam model. Also, in appendix B, as a by-product of this work, the instrumental effects of the NRAO 91 meter telescope are quantified, and possible causes of the instrumental effects are discussed.

II. Model Theory

The present theoretical model is based on the work of Imbriale *et al* (1974). They derived a scalar approximation for the far zone electric field pattern of a parabolic reflector system in which the receiver feed position may undergo large lateral displacements. This scalar approximation requires that the E and H plane feed illumination patterns be symmetric, and that the incident radiation not be blocked from the telescope reflector. However, the NRAO 6 cm dual feed system illumination pattern is asymmetric and the 91 meter radio telescope feed legs partially block incident radiation from the reflector. To account for the asymmetric feed illumination and the blockage, the work of Imbriale *et al* is developed further in this thesis.

Using the approximations [that the feed illumination pattern is fixed with respect to the reflector coordinates, that the feed displacement is accounted for only in the electric field phase, and that the observation point (θ, ϕ) is within approximately eight wavelengths of the boresight (see Figure 1)], Imbriale *et al* derived the scalar approximation for the far zone electric field $E(\theta, \phi)$. Thus

$$E(\theta,\phi) = \frac{-ika^2 \exp(-ik(2f+R))}{4\pi R f} \cdot \int_0^1 \exp(ik\epsilon_z \cos\theta') I(r)(1-\cos\theta') r\, dr \qquad (1)$$

where

$$I(r) = \int_0^{2\pi} (\sin^2\phi' E_p + \cos^2\phi' H_p) \exp(ikar \sin\theta \cos(\phi - \phi')) \cdot \exp(ik(\epsilon_x \sin\theta' \cos\phi' + \epsilon_y \sin\theta' \sin\phi'))\, d\phi',$$

$$\cos\theta' = \frac{a^2r^2 - 4f^2}{a^2r^2 + 4f^2} \qquad (2),$$

$i = \sqrt{-1}$, $k = 2\pi/\lambda$, λ is the electric field wavelength, f is the telescope focal length, R is the distance to the point (θ, ϕ), a is the telescope radius, ϵ_x is the x direction feed displacement, ϵ_y is the y direction feed displacement, ϵ_z is the z direction feed displacement, r is a dimensionless radial integration parameter defined by equation 2, ϕ' is the azimuthal angle integration parameter, θ' is the polar angle integration parameter,

E_p is the complex far zone electric field amplitude in the E plane, and H_p is the complex far zone electric field amplitude in the H plane (see Figure 2).

In this thesis the feed illumination asymmetry and blockage are added to the theoretical beam model $E(\theta,\phi)$ of Imbriale *et al* by expanding E_p and H_p within $I(r)$. The feed illumination asymmetry in the E and H planes are represented as E_p^+ and E_p^-, and as H_p^+ and H_p^- respectively. Furthermore the feed illumination blockage is simply characterized by zeroing the incident field wherever it is blocked. In the case of the 91 meter telescope the feed legs lie in the $y = 0$ plane, hence the blockage is characterized by L, the feed leg width (see Figure 3). Thus by the addition of asymmetry and blockage the incident feed illumination is characterized as

$$E_p = \begin{cases} E_p^+, & \text{for} \quad \Delta\phi < \phi' < \pi - \Delta\phi; \\ E_p^-, & \text{for } \pi + \Delta\phi < \phi' < 2\pi - \Delta\phi; \\ 0, & \text{elsewhere.} \end{cases}$$

$$H_p = \begin{cases} H_p^+, & \text{for} \quad \Delta\phi < \phi' < \frac{\pi}{2}; \\ H_p^-, & \text{for} \quad \frac{\pi}{2} < \phi' < \pi - \Delta\phi; \\ H_p^-, & \text{for } \pi + \Delta\phi < \phi' < \frac{3\pi}{2}; \\ H_p^+, & \text{for} \quad \frac{3\pi}{2} < \phi' < 2\pi - \Delta\phi; \\ 0, & \text{elsewhere.} \end{cases}$$

where $\Delta\phi = \arcsin\left(\frac{L}{2a}\right)$. The solution to $I(r)$ (determined by inserting the incident feed illumination and then integrating) is an infinite sum of integer order Bessel functions. The complete solution is

$$\begin{aligned} I(r) = J_0(\omega)\left[\frac{E_p^+ + E_p^- + H_p^+ + H_p^-}{2}(\pi - 2\Delta\phi) + \frac{E_p^+ + E_p^- - H_p^+ - H_p^-}{2}\sin(2\Delta\phi)\right] \\ + i\sum_{m=0}^{\infty} J_{2m+1}(\omega)(-1)^m\left[(E_p^+ - E_p^-)\sin(2m+1)\beta\left(\frac{2\cos(2m+1)\Delta\phi}{2m+1}\right.\right. \\ \left. - \frac{\cos(2m+3)\Delta\phi}{2m+3} - \frac{\cos(2m-1)\Delta\phi}{2m-1}\right) \\ + (H_p^+ - H_p^-)\cos(2m+1)\beta\left(\frac{2(-1)^m - \sin(2m+1)\Delta\phi}{2m+1}\right. \\ \left.\left. + \frac{(-1)^{m+1} - \sin(2m+3)\Delta\phi}{2m+3} + \frac{(-1)^{m+1} - \sin(2m-1)\Delta\phi}{2m-1}\right)\right] \end{aligned}$$

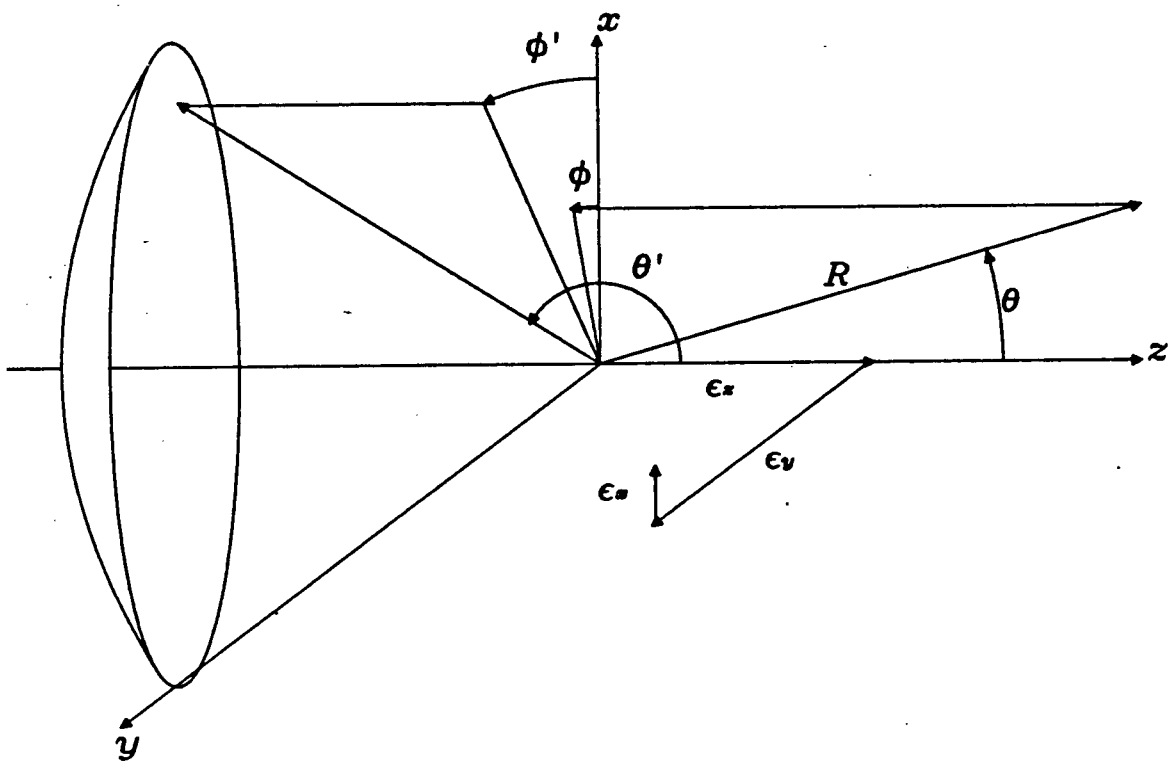

Figure 1. Diagram of the telescope coordinate system (model coordinates). The origin corresponds to the focal point of the telescope.

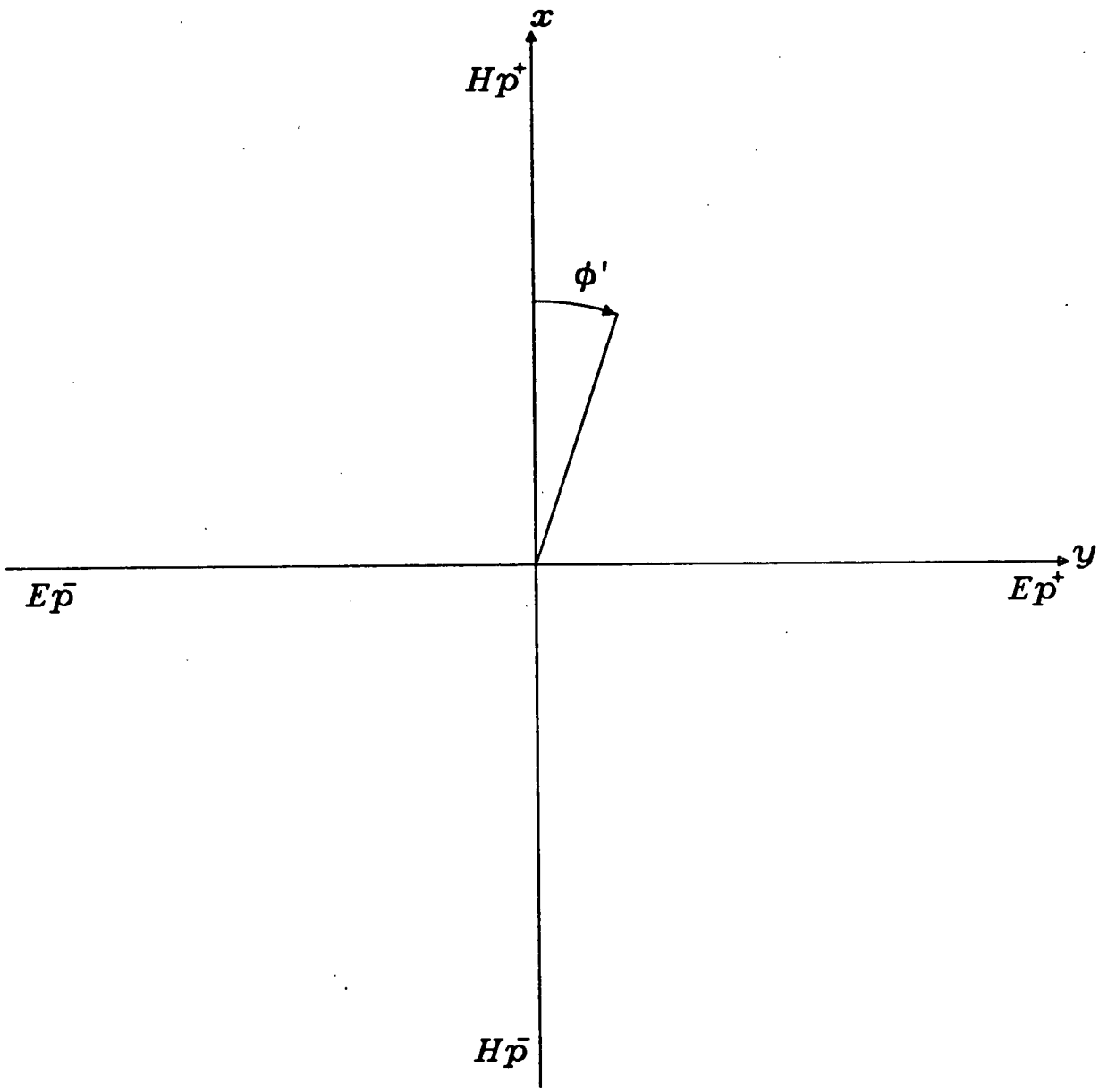

Figure 2. Diagram of the E_p^+, E_p^-, H_p^+, and H_p^- electric field components in the model coordinate system. The θ' coordinate, which describes the angular dependence of E_p^+, E_p^-, H_p^+, and H_p^-, is perpendicular to the ϕ' coordinate.

$$+\sum_{n=1}^{\infty} J_{2n}(\omega)(-1)^n \cos 2n\beta \left[\frac{E_p^+ + E_p^- + H_p^+ + H_p^-}{2} \frac{(-\sin 2n\Delta\phi)}{n} \right.$$

$$+ \frac{E_p^+ + E_p^- - H_p^+ - H_p^-}{4} \left(\frac{\sin 2(n+1)\Delta\phi}{n+1} \right.$$

$$\left. \left. + \frac{\sin 2(n-1)\Delta\phi - \sin 2(n-1)(\pi - \Delta\phi)}{2(n-1)} \right) \right]$$

where

$$\omega = k \sin\theta' ((\epsilon_x + \rho \sin\theta \cos\phi)^2 + (\epsilon_y + \rho \sin\theta \sin\phi)^2)^{1/2},$$

$$\tan\beta = \frac{\epsilon_y + \rho \sin\theta \sin\phi}{\epsilon_x + \rho \sin\theta \cos\phi}, \text{ and } \quad \rho = \frac{ar}{\sin\theta'}.$$

Fortunately the $I(r)$ series converges rapidly so that it is approximated by truncating the series after the fourth order Bessel function (accurate to 0.1% of the peak). Inserting $I(r)$ into equation (1) reduces $E(\theta, \phi)$ to a one dimension integral. Because this integral is intractable it is solved by numerical integration. Thus $E(\theta, \phi)$ represents the scalar approximation of the far zone electric field at point (θ, ϕ) for one receiver feed. The differential beam of the 6 cm dual feed system is modeled by

$$B(\theta, \phi) = E_{(A)} \cdot E^*_{(A)} - E_{(B)} \cdot E^*_{(B)}$$

where $E_{(A)}$ and $E_{(B)}$ are the far zone complex electric field amplitudes of feeds A and B respectively. Thus the theoretical beam model $B(\theta, \phi)$ accounts for the asymmetric feed illumination of the 6 cm dual feed system and the incident radiation blockage of the 91 meter radio telescope.

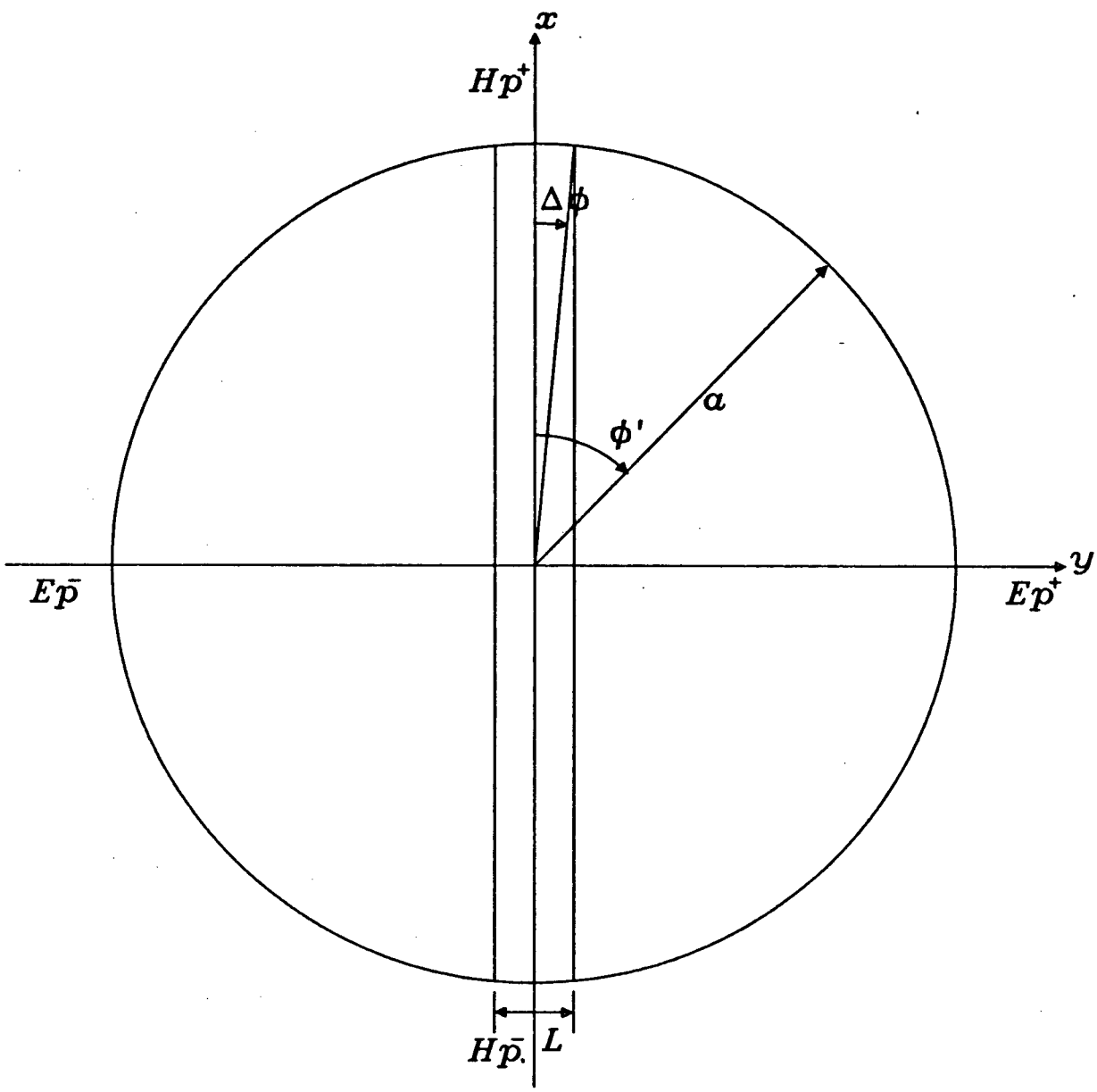

Figure 3. Diagram of the feed leg blockage in the model coordinate system.

III. Model Parameters

As shown previously, the theoretical beam model requires several parameters to specify the parabolic reflector dimensions, the feed illumination patterns, and the feed horn locations. All these parameters were derived from information provided by the National Radio Astronomy Observatory.

The 91 meter telescope, located at a latitude of $38^\circ\,25'\,46.3''$, is a meridian transit instrument. The physical characteristics used in the theoretical model to describe the parabolic reflector are the reflector radius a, the focal length f, and the feed leg width L which are 45.72 meters, 38.735 meters, and 2.13 meters respectively. Although the feed legs are a lattice structure, in this analysis they are assumed to block incident radiation completely

For the phase I Galactic Radio Patrol work the dual channel 6 cm cooled GaAsFet receiver and sectorial feed system were located at the telescope focus. The 6 cm receiver was operated at a center frequency of 4.75 GHz with a bandwidth of 580 MHz. Thus the theoretical model assumes that the observational wavelength λ is 6.32 cm.

The feed horn consists of two sectorial horns fixed together. Measurements of the feed horn electric field amplitude and phase patterns were obtained from Dr. J. R. Fisher of NRAO (see Figures 4, 5, 6, 7, 8, and 9). The E and H plane electric field amplitude patterns of both feeds were measured at the receiver center frequency. Unfortunately the E and H plane electric field phase patterns had not been measured for the dual 6 cm feed system; instead, the E and H plane phase patterns had been measured on a geometrically scaled version of the 6 cm feed horn. On the assumption that the scaled feed horn electric field phase patterns are not significantly different from the 6 cm phase patterns, the scaled feed horn phase patterns were used.

The most significant theoretical model parameters are the feed horn positions. In

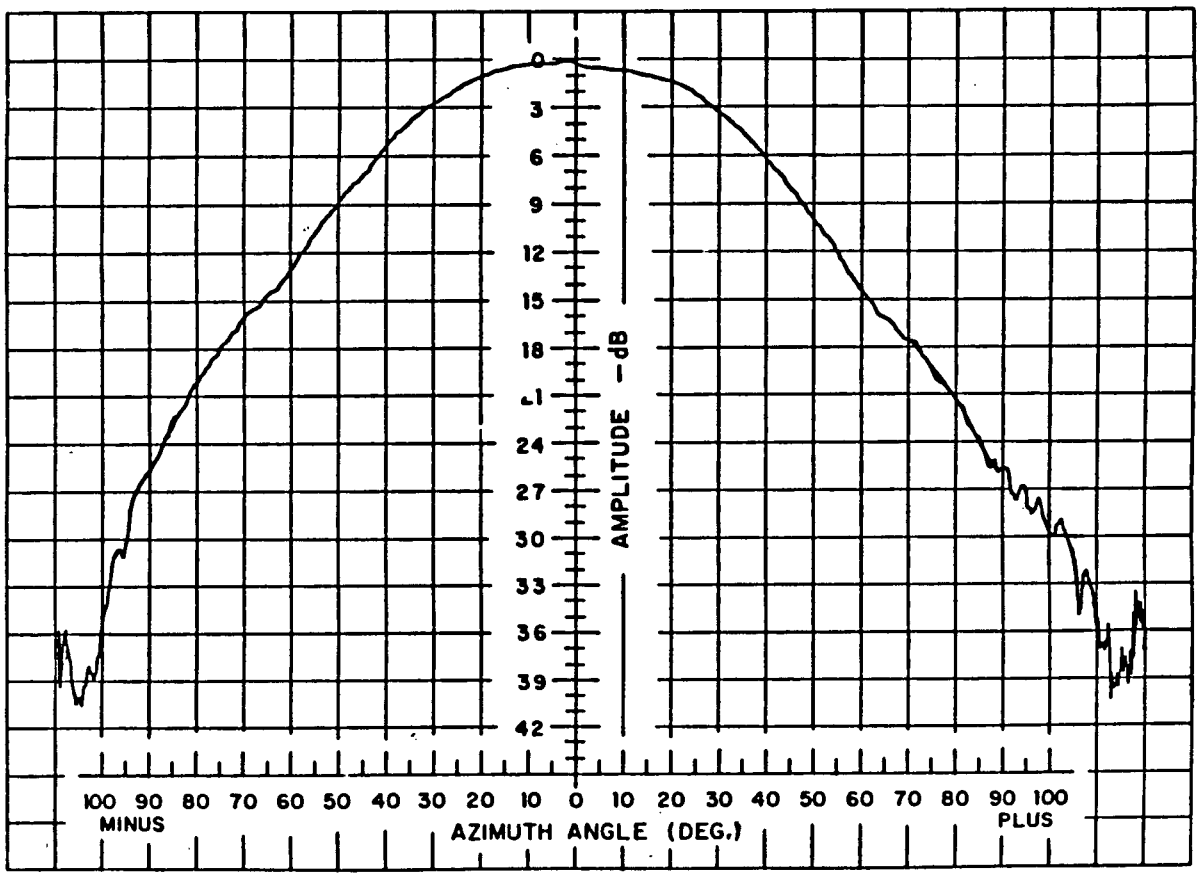

Figure 4. Diagram of feed A E plane electric field amplitude pattern measured at 4.75 GHz. The azimuth angle axis corresponds to θ' the polar angle in this analysis (J. R. Fisher private communication).

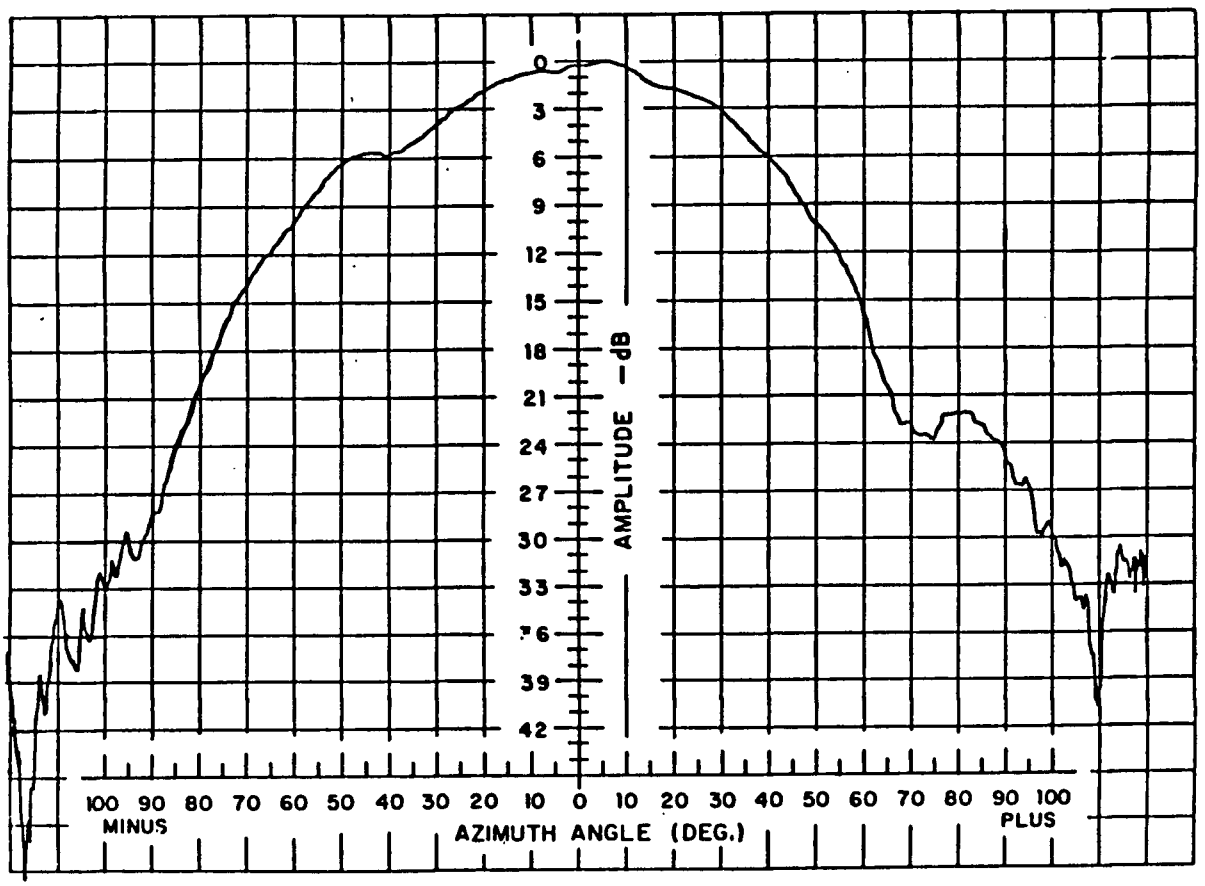

Figure 5. Diagram of feed A H plane electric field amplitude pattern measured at 4.75 GHz. The azimuth angle axis corresponds to θ' the polar angle in this analysis (J. R. Fisher private communication).

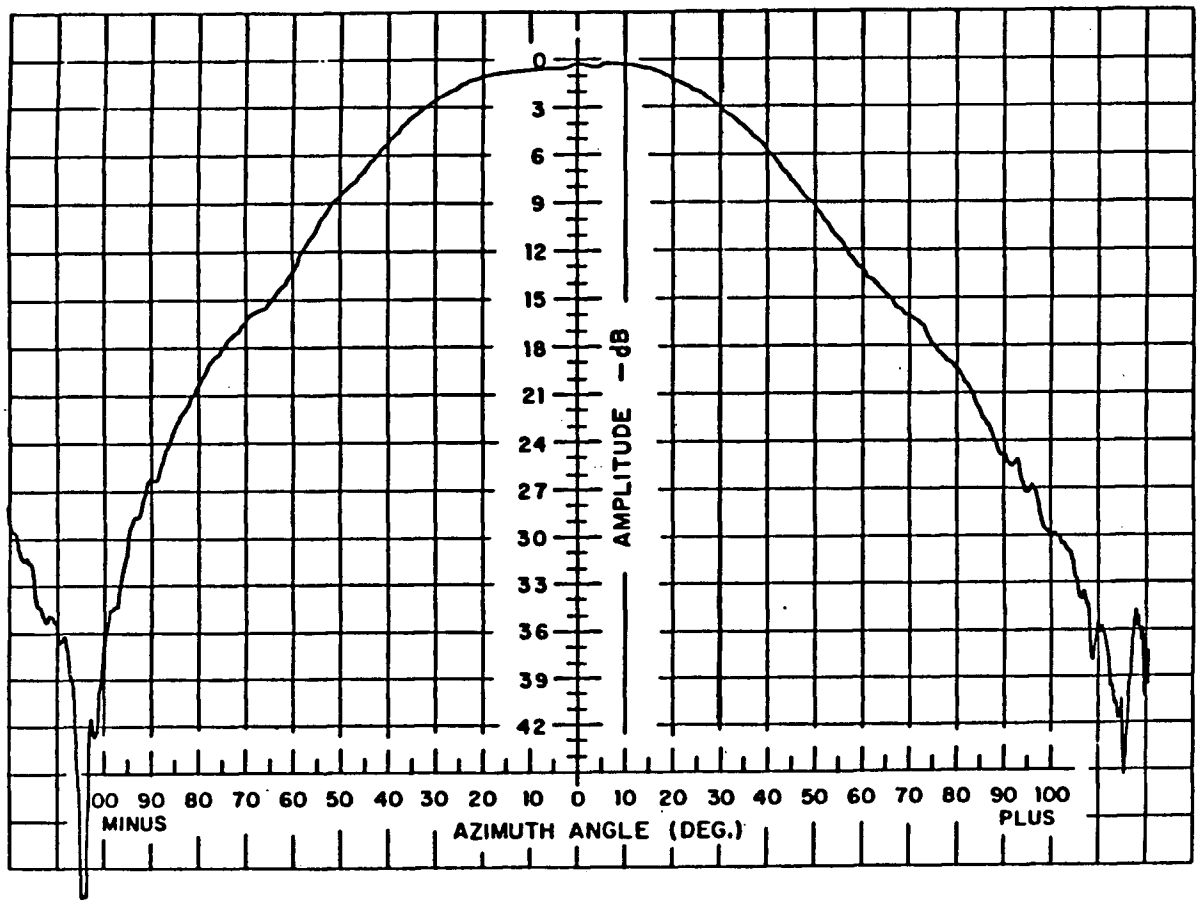

Figure 6. Diagram of feed B E plane electric field amplitude pattern measured at 4.75 GHz. The azimuth angle axis corresponds to θ' the polar angle in this analysis (J. R. Fisher private communication).

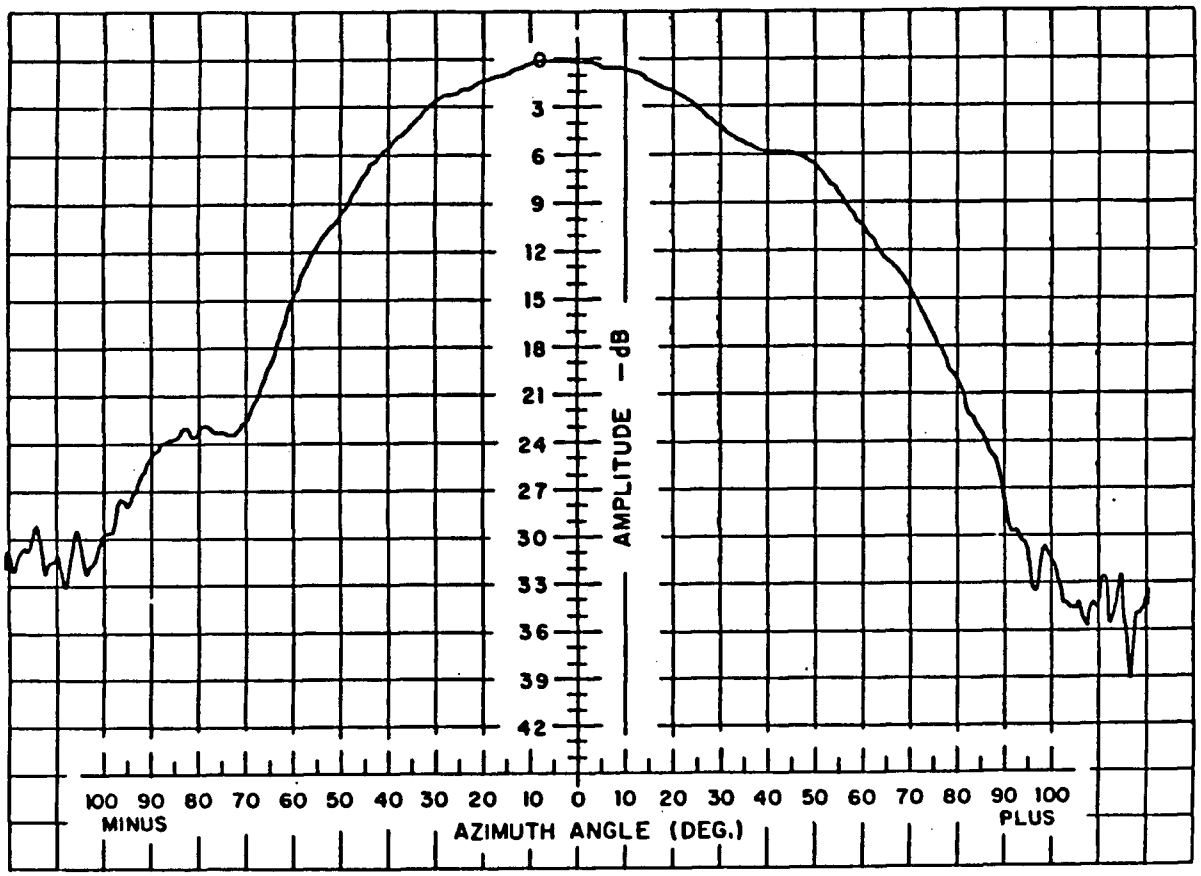

Figure 7. Diagram of feed B H plane electric field amplitude pattern measured at 4.75 GHz. The azimuth angle axis corresponds to θ' the polar angle in this analysis (J. R. Fisher private communication).

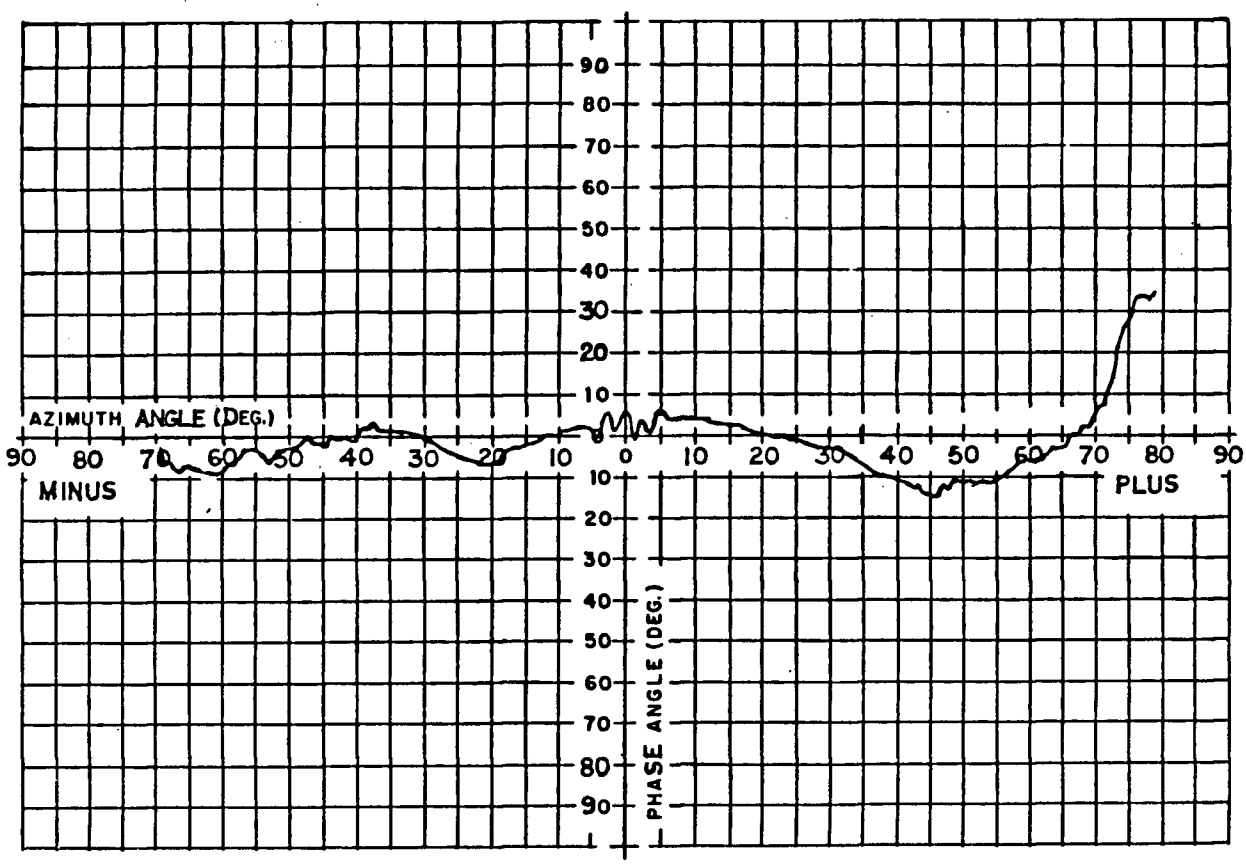

Figure 8. Diagram of the E plane electric field phase pattern measured at the center frequency on a scaled feed horn. The azimuth angle axis corresponds to θ' the polar angle in this analysis (J. R. Fisher private communication).

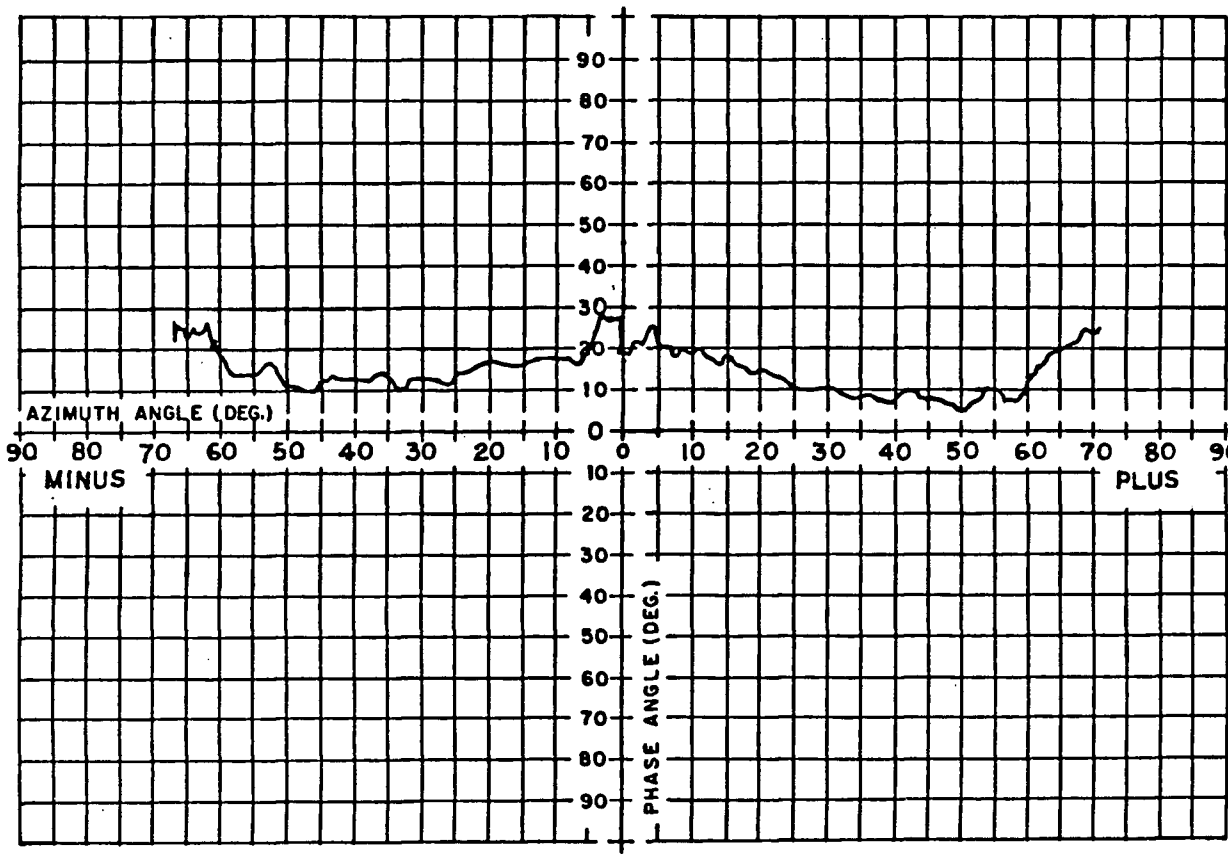

Figure 9. Diagram of the H plane electric field phase pattern measured at the center frequency on a scaled feed horn. The azimuth angle axis corresponds to θ' the polar angle in this analysis (J. R. Fisher private communication).

particular the theoretical model seems to be more sensitive to the feed horn displacement within the telescope focal plane than to the displacement perpendicular to the focal plane. This result corresponds to the findings of the work done to determine the best receiver focus position of the 91 meter telescope (Fisher and Payne 1982). For these reasons the theoretical model assumes that the feed horn z displacement ϵ_z is zero.

The feed horn position in the focal plane is determined by three factors. First the feed horns are a fixed 9.413 cm apart. Second the feed horns are mounted on a turntable that rotates, accurate to one degree, about the center point between the two feeds. Third there is an instrumental effect caused by the gravitational deformation of the telescope reflecting dish. Specifically J. R. Fisher and H. E. Payne discovered, after observing several sources over a range of declinations and feed horn positions, that the best reflector focus position changed in the north-south direction at a rate of .74 cm per degree from the telescope zenith (see Figure 10). Conversely this work assumes that the feed horn positions change while the best telescope focus point remains fixed. With the above constraints on the feed horn dimensions and movements the feed horn positions used by the theoretical model are

$$\epsilon_x = -.0470635 \cos(RT) - .0074(Z - \delta) \quad \text{meters}$$

$$\epsilon_y = -.0470635 \sin(RT) \quad \text{meters}$$

for feed A and

$$\epsilon_x = +.0470635 \cos(RT) - .0074(Z - \delta) \quad \text{meters}$$

$$\epsilon_y = +.0470635 \sin(RT) \quad \text{meters}$$

for feed B, where RT is the feed horn system rotation angle, δ is the telescope declination, and Z is the telescope latitude. It should be noted that the parameters derived here are not obtained from the calibration data. Rather the model calibration section discusses the adjustments made to these model parameters to improve the fit of the theoretical beam model to the calibration data.

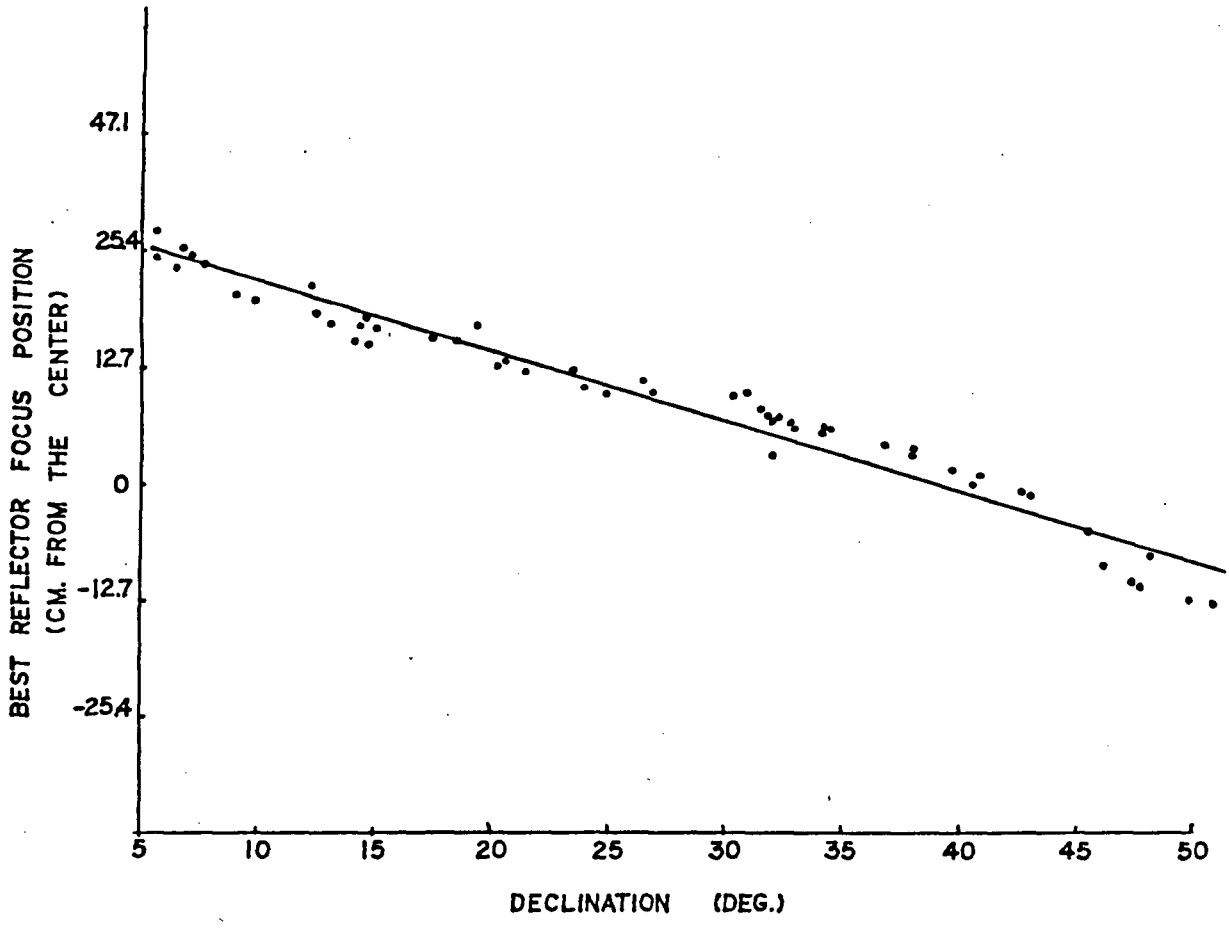

Figure 10. Plot of the best reflector focus position versus the declination of the telescope. The points correspond to the observed data and the line indicates a slope of .74 cm per degree from the telescope zenith (J. R. Fisher private communication).

IV. Coordinates

Before the theoretical model can be calibrated by the observed data or used to deconvolve the observed data, one must be able to transform a point in the equatorial coordinate system (α, δ) to a point in the theoretical model coordinate system (θ, ϕ) (see Figures 11 and 12). All points in the equatorial system are called data coordinates, and all points in the theoretical model system are called model coordinates. The differential beam center point is defined as the point equally spaced between the two main lobes of the differential beam (see Figure 11). The telescope is calibrated so that the coordinates (α_c, δ_c) ascribed to each data point indicate the location of the differential beam center when the data point is measured. In the model coordinates the beam center point is (θ_c, ϕ_c) (see Appendix A). Thus the data coordinates (α_c, δ_c) always correspond to the model coordinates (θ_c, ϕ_c) and vice versa.

The transformation from data coordinates to model coordinates relies on the two assumptions that the telescope y axis points due west in the equatorial coordinate system, and that the z axis coordinates (α_z, δ_z) in the equatorial system are known. With these two assumptions the transformation from data coordinates (α, δ) to model coordinates (θ, ϕ) is

$$\sin\theta\cos\phi = \sin\delta\cos\delta_z - \sin\delta_z\cos\delta\cos(\alpha_z - \alpha) \tag{1}$$

$$\sin\theta\sin\phi = \cos\delta\sin(\alpha_z - \alpha) \tag{2}$$

$$\cos\theta = \sin\delta_z\sin\delta + \cos\delta_z\cos\delta\cos(\alpha_z - \alpha) \tag{3}$$

where (α_z, δ_z) are the z axis coordinates in the equatorial system.

Because the feed horns are displaced in the telescope focal plane, the coordinates (α_z, δ_z) are not usually known. However (α_z, δ_z) can be determined from the corresponding beam center points (α_c, δ_c) and (θ_c, ϕ_c). Using the fact that (α, δ) corresponds to (θ, ϕ) when (α_z, δ_z) is known in equations (1), (2), and (3) one sets $(\alpha, \delta) = (\alpha_c, \delta_c)$ and

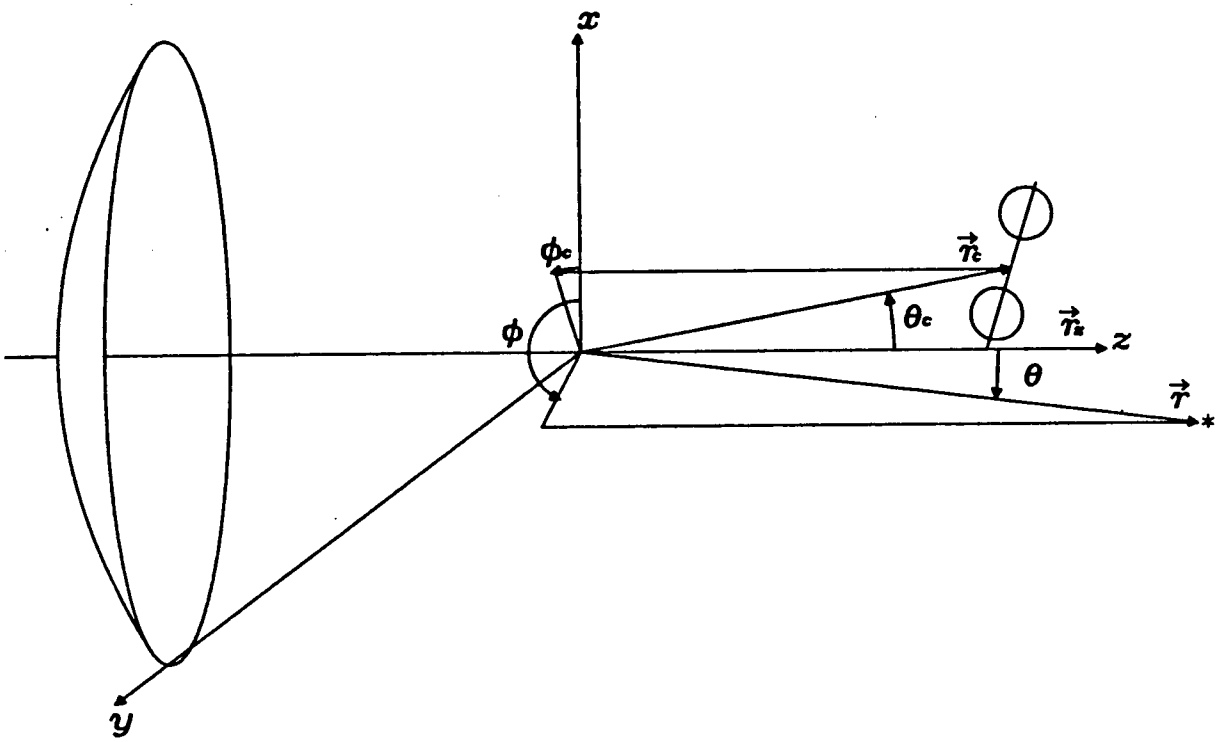

Figure 11. Diagram of the model coordinates where $\vec{r_c} = (\theta_c, \phi_c)$, $\vec{r_z} = z$ axis, and $\vec{r} = (\theta, \phi)$.

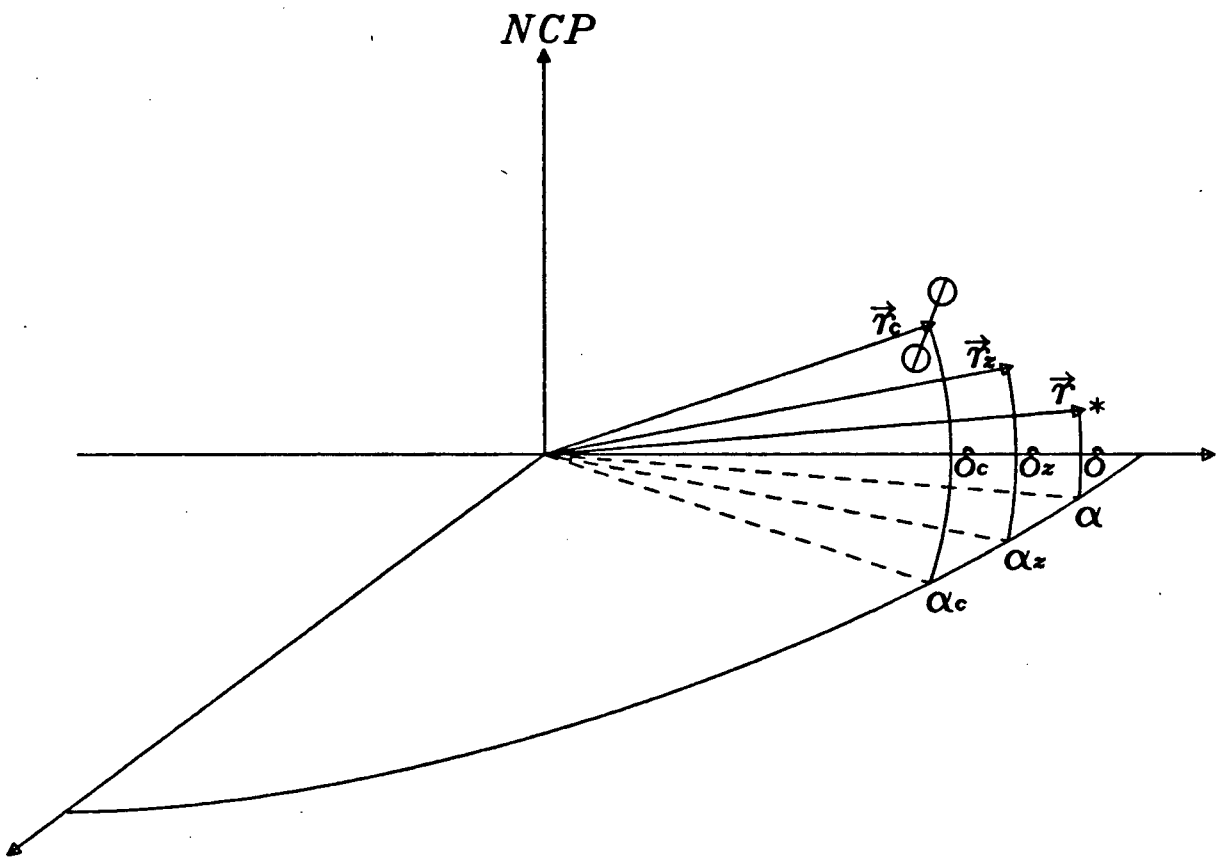

Figure 12. Diagram of the data coordinates where $\vec{r_c} = (\alpha_c, \delta_c)$, $\vec{r_z} = (\alpha_z, \delta_z)$, and $\vec{r} = (\alpha, \delta)$.

$(\theta, \phi) = (\theta_c, \phi_c)$ in these equations and then inverts the equations to solve for (α_z, δ_z). The solution to (α_z, δ_z) is

$$\alpha_z = \alpha_c + \arcsin\left(\frac{\sin\theta_c \sin\phi_c}{\cos\delta_c}\right) \tag{4}$$

$$\cos\delta_z = \frac{\cos\theta_c \cos\delta_c \cos(\alpha_z - \alpha_c) + \sin\delta_c \sin\theta_c \cos\phi_c}{\cos^2(\alpha_z - \alpha_c)\cos^2\delta_c + \sin^2\delta_c} \tag{5}$$

$$\sin\delta_z = \frac{\sin\delta_c \cos\delta_z - \sin\theta_c \cos\phi_c}{\cos\delta_c \cos(\alpha_z - \alpha_c)} \tag{6}$$

Now that the point (α_z, δ_z) is determined, one can transform from data coordinates (α, δ) to model coordinates (θ, ϕ) using equations (1), (2), and (3). Thus the observed data can be reliably compared to the theoretical beam model.

V. Calibration

After the information from the NRAO had been used to estimate the theoretical beam model parameters, point source data were used to calibrate the model further. In fact, to improve the accuracy of the beam model, three more parameters had to be added to the model. Also, during the model calibration, significant differences between the observed beam and the theoretical beam indicate that there are instrumental effects reducing the telescope performance. Possible causes of these problems were analyzed with the hope that the telescope performance would be improved, or at least be quantified.

Fourteen point sources were observed at three declination drive rates and three beam rotation angles (see Table I). The telescope was driven in declination along its meridian at $120'/min$, $60'/min$ and $0'/min$ (drift). Of course since the telescope is a transit instrument, the $15' \cos \delta/min$ rotation of the earth was added to the telescope's motion. Also the beam was rotated so that different parts of the beam were observed by each scan. In total four types of calibration sources were used. The scans observed at $120'/min$ declination drive rate were observed during the nighttime, and the scans observed at the other drive rates were observed during the daytime. The theoretical beam model was calibrated within the declination range $23° \leq \delta \leq 62°$, since outside this range few strong point sources were observed and the data and the model differed by more than 3% of the beam peak. Throughout this work, data observed at 90° beam rotation to the telescope meridian and $0'/min$ declination drive rate are called 90°-drift data, data observed at 0° beam rotation to the telescope meridian and $0'/min$ declination drive rate are called 0°-drift data, data observed at 0° beam rotation to the scan track and $60'/min$ declination drive rate are called $0° - 60'/min$ driven data, and data observed at 11° beam rotation to the scan track and $120'/min$ declination drive rate are called $11° - 120'/min$ driven data.

As one of the main reasons for this work was to derive a telescope beam model

Table I.

Numbers of Scans per Point Source

Source Name	δ_{1950}	α_{1950}	Flux (Jansky)	0° drift	90° drift	0° $60'/min$	11° $120'/min$
3C165	$23°22'8''$	$6^h40^m4.9^s$	0.77±.03				4
3C287	$25°24'37''$	$13^h28^m15.96^s$	3.26±.06	5	1		
1829+290	$29°4'57''$	$18^h29^m17.94^s$	1.15±.04	5	1	1	
3C131	$31°24'32''$	$4^h50^m10.55^s$	0.86±.04				4
3C236	$35°8'48''$	$10^h3^m5.39^s$	1.34±.08	6	1	1	
DA267	$39°15'24''$	$9^h23^m55.29^s$	7.57±.13	6	1	1	
NGC7027	$42°21'3''$	$21^h5^m9.39^s$	5.44±.05				3
3C388	$45°30'22''$	$18^h42^m35.49^s$	1.77±.04	5	1	1	
3C349	$47°7'9''$	$16^h58^m5.06^s$	1.14±.04	5	1		
3C196	$48°22'7''$	$8^h9^m59.42^s$	4.36±.06	6	1	1	
3C295	$52°26'13''$	$14^h9^m33.5^s$	6.53±.08	5	1	1	
3C52	$53°17'46''$	$1^h45^m14.9^s$	1.48±.06				4
DA251	$55°44'42''$	$8^h31^m4.38^s$	5.60±.06	6	1	1	
1358+624	$62°25'8''$	$13^h58^m58.3^s$	1.77±.02	4		1	

accurate to 3% of the beam peak, the sources chosen to calibrate the theoretical model had to have a high flux density so that the receiver noise was less than 1% of the peak of the scan. In general, sources with flux density greater than 1.0 Jansky were selected. However two point sources with a flux density less than 1.0 Jansky, observed at $120'/min$ drive rate, were used because there were so few scans at this drive rate. Their noise was reduced by the averaging of repeated observations. The receiver noise, ΔT_{rms}, follows the derivation of M.E. Tuiri (1964),

$$\Delta T_{rms} = \frac{K_s T_{sys}}{\sqrt{\Delta\nu_{HF}\, t_{LF}}}$$

where the receiver constant $K_s = 2$, the receiver system temperature $T_{sys} = 70$ K and the receiver bandwidth $\Delta\nu_{HF} = 580$ MHz. The equivalent integration time t_{LF} is related to the integration time t by the relation

$$t_{LF} = \frac{t}{1.57}.$$

The $11° - 120'/min$ and $0° - 60'/min$ driven data have an integration time of .2 seconds whereas the 0°-drift and 90°-drift data have an integration time of 1.0 seconds. Conse-

quently for each receiver $\Delta T_{rms} = 16.3$ mK for the driven data and $\Delta T_{rms} = 7.3$ mK for the drift data. Each scan is the average of two receivers so that the noise is reduced by $\sqrt{2}$. Furthermore the $11^\circ - 120'/min$ driven data were observed n times reducing the noise further by $\sqrt{n}$. Analysis of the receiver noise showed it to be less than 1% of the peak of each scan. Finally it should be noted that pointing corrections, based on the $0^\circ - 60'/min$ driven data and the 90°-drift data (Taylor 1982), were added to the coordinates of each data scan.

Two processes are involved in calibrating the theoretical beam model with the point source data. First iterative methods were used to find the beam model parameters which cause the model best to fit the observed data. The iterative methods used for each type of scan are discussed in detail below. The second process quantifies the fit of the beam model to the observed data by directly comparing the model to the data.

The method used to compare the theoretical beam model to the point source data was the same for all types of scan data. Because the beam model needs only to predict the relative intensity and positioning of the beam, both the observed data and the theoretical model were normalized by their peak point value, and the theoretical model was shifted until its peak point position coincided with the observed data peak point position. It is important to note that because of noise at the data beam peaks, the peak point position was determined as the average of the half power beam width positions from either side of the beam. After the model and data scans were normalized and the model peak position shifted, graphs of the theoretical beam superimposed on the observed beam and graphs of the residual difference between the theoretical beam model and the observed beam were plotted. These graphs provided information on the accuracy of the theoretical beam model.

The most accurate calibration data are the drift scan data. First it is necessary to consider the calibration of the model to the 90°-drift scan data. The scan track in

the 90°-drift data is parallel to a line joining both beam A and beam B (called the main axis). Consequently a typical 90°-drift scan has a positive lobe and a negative lobe corresponding to feed A and feed B (see Figure 13). Initial comparison of the theoretical model to the 90° drift data showed that the model did not fit the data. Detailed analysis shows that the observed data peak ratio, $\frac{peakA}{peakB}$, is 5% greater than the theoretical model peak ratio. This suggested that the model feed position parameters were wrong. The theoretical model peak ratio is most sensitive to a y direction change in the feed horn position. Therefore a y shift parameter Δy was added to the feed horn position equations. Another problem with the theoretical model is that the observed data separation between peak points is greater than the theoretical model separation between peak points. To fit the 90°-drift data a feed separation factor EX was added to the feed horn position equations. Originally the ϵ_z parameter was varied to account for the peak point separation; however, this reduced the accuracy of the fit of the model to the data. With the addition of Δy and EX the feed horn positions equations became

$$\epsilon_x = -.0470635\ EX \cos(RT) - .0074\ (Z - \delta) \quad \text{meters}$$

$$\epsilon_y = -.0470635\ EX \sin(RT) + \Delta y \quad \text{meters}$$

for feed A and,

$$\epsilon_x = +.0470635\ EX \cos(RT) - .0074\ (Z - \delta) \quad \text{meters}$$

$$\epsilon_y = +.0470635\ EX \sin(RT) + \Delta y \quad \text{meters}$$

for feed B.

Simple iteration methods were derived to determine the Δy and EX parameters for the 90°-drift data. For small values the Δy parameter is assumed to be linearly related to the beam peak ratio. Also, since the Δy parameter is determined once the model beam peak ratio equals the observed data peak ratio, the two previous estimates for Δy and the corresponding model beam peak ratios are used to linearly interpolate a new Δy value. It can be shown that

$$\Delta y_3 = \left(\frac{PRM_1}{PRD}\right)\left(\frac{PRM_2 - PRD}{PRM_1 - PRM_2}\right)(\Delta y_2 - \Delta y_1) + \Delta y_2$$

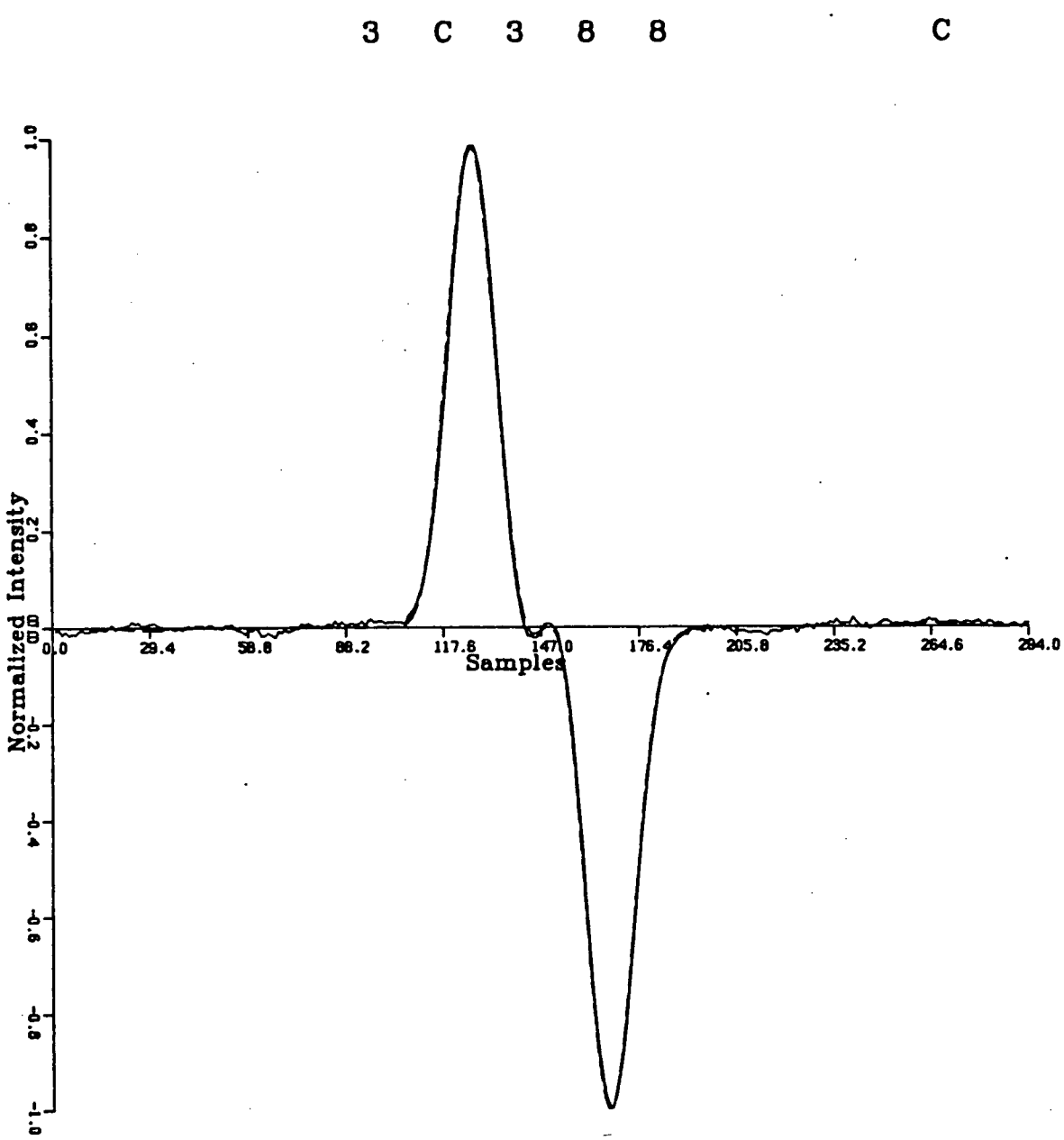

Figure 13. Plot of the final theoretical beam model (dashed lines) superimposed on a 90°-drift scan through the source 3C388.

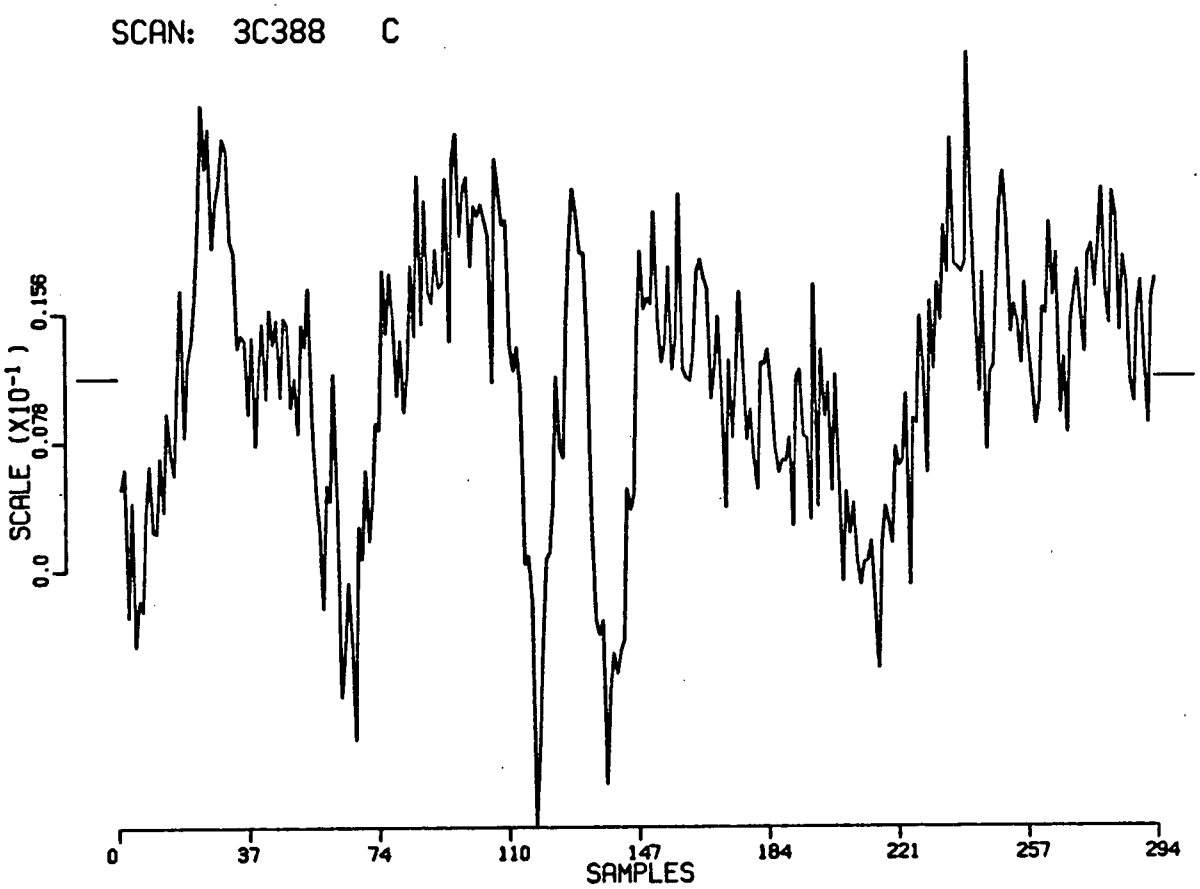

Figure 14. Plot of the residuals between the final theoretical beam model and the 90°-drift scan through the source 3C388. The maximum residual is 2.5% of the beam peak.

where the new y shift parameter, Δy_3, is determined from the two previous shift parameters, Δy_1 and Δy_2, the observed data peak ratio, PRD, and the two previous theoretical model peak ratios, PRM_1 and PRM_2. The EX parameter is directly proportional to the beam peak separation. The new separation factor, EX_2, is determined from the previous separation factor, EX_1, the previous theoretical model peak separation, SM_1, and the observed data peak separation, SS, by the relation

$$EX_2 = \left(\frac{SS}{SM_1}\right) EX_1 .$$

When the Δy parameter changes by less than 1% (after approximately 6 iterations), the Δy and EX parameters have converged. The average peak residual of all the 90°-drift scans is 3.7%. Because the parameters derived for each source are relatively constant, the average parameter values $\Delta y = -0.022$ meters and $EX = 1.01$ are used by the beam model to fit the 90°-drift data. Since the 90°-drift scan data are its most sensitive measurement, the Δy parameter is fixed at -0.022 meters for the rest of this work. The final theoretical model fit to the data for the source 3C388 is shown in figure 13 and the residuals are shown in figure 14.

0°-drift scans were used independently to check the Δy and EX parameter values derived from the 90°-drift scans. The 0°-drift scan track is perpendicular to the main beam axis. Thus a typical 0°-drift scan shows either a positive or a negative main lobe due either to feed A or feed B respectively (see Figure 15). Between four and six separate 0°-drift scans, offset by one arcminute, were observed for each source. Residuals between the data and the model were found for each 0° -drift scan. The peak residuals for each source were averaged to give the average peak residual for a source. These values were averaged again to give the average peak residual for the 0°- drift data which is 2.8% of the beam peak. The final theoretical model fits to the data for the source DA267 are shown in figures 15, 17, 19, 21, 23, and 25 and the residuals are shown in figures 16, 18, 20, 22, 24, and 26. Thus the 0°-drift data, which consist of several offset scans through

the same source, provide good independent confirmation that the theoretical beam model using $\Delta y = -0.022$ meters and $EX = 1.01$ describes the observed drift scan beam to the 3% level of the beam peak.

Next the theoretical beam model was calibrated by the driven declination point source data. The $0° - 60'/min$ data scan track was parallel to the beam main axis. Thus a typical $0° - 60'/min$ data scan has a positive and negative lobe corresponding to feed A and feed B (see Figure 27). The initial work calibrating the theoretical model with the $0° - 60'/min$ data showed that the data scans are much broader than the model even after allowing for the expected broadening due to the 0.2^s integration time of the data. The theoretical model parameters could not account for the $0° - 60'/min$ data broadening. It seemed that the best way to fit the theoretical beam model to the $0° - 60'/min$ data was to convolve the theoretical model with a 1 dimensional gaussian of half power beamwidth H in the declination direction, using the assumption that the broadening is caused by the declination drive motor shaking the receiver feeds at a high frequency. Thus a third parameter H, the gaussian halfpower beamwidth, was added to the theoretical beam model. Because the H parameter is determined once the model beam HPBWs equal the observed data HPBWs, two previous estimates for H and the corresponding model beam HPBWs are used to linearly interpolate a new H value. The iteration formula used to find H, which is similar to the formula used to determine Δy, is

$$H_3 = \left[\left(\frac{HAM_1}{HAD}\right)\left(\frac{HAM_2 - HAD}{HAM_1 - HAM_2}\right) + \left(\frac{HBM_1}{HBD}\right)\left(\frac{HBM_2 - HBD}{HBM_1 - HBM_2}\right)\right]\frac{(H_2 - H_1)}{2} + H_2$$

where H_3 is the new gaussian HPBW, H_1 and H_2 are the two previous estimates of the gaussian HPBWs, HAM_1 and HAM_2 are the two previous model A beam HPBWs, HBM_1 and HBM_2 are the two previous model B beam HPBWs, HAD is the observed data A beam HPBW, and HBD is the observed data B beam HPBW. The EX parameter was iterated the same way as was done in the 90°-drift data, and the Δy parameter was set equal to -0.022 meters. Because the parameters derived for each source are relatively constant, the average parameter values EX =1.01 and $H = 89''$ were used by the beam

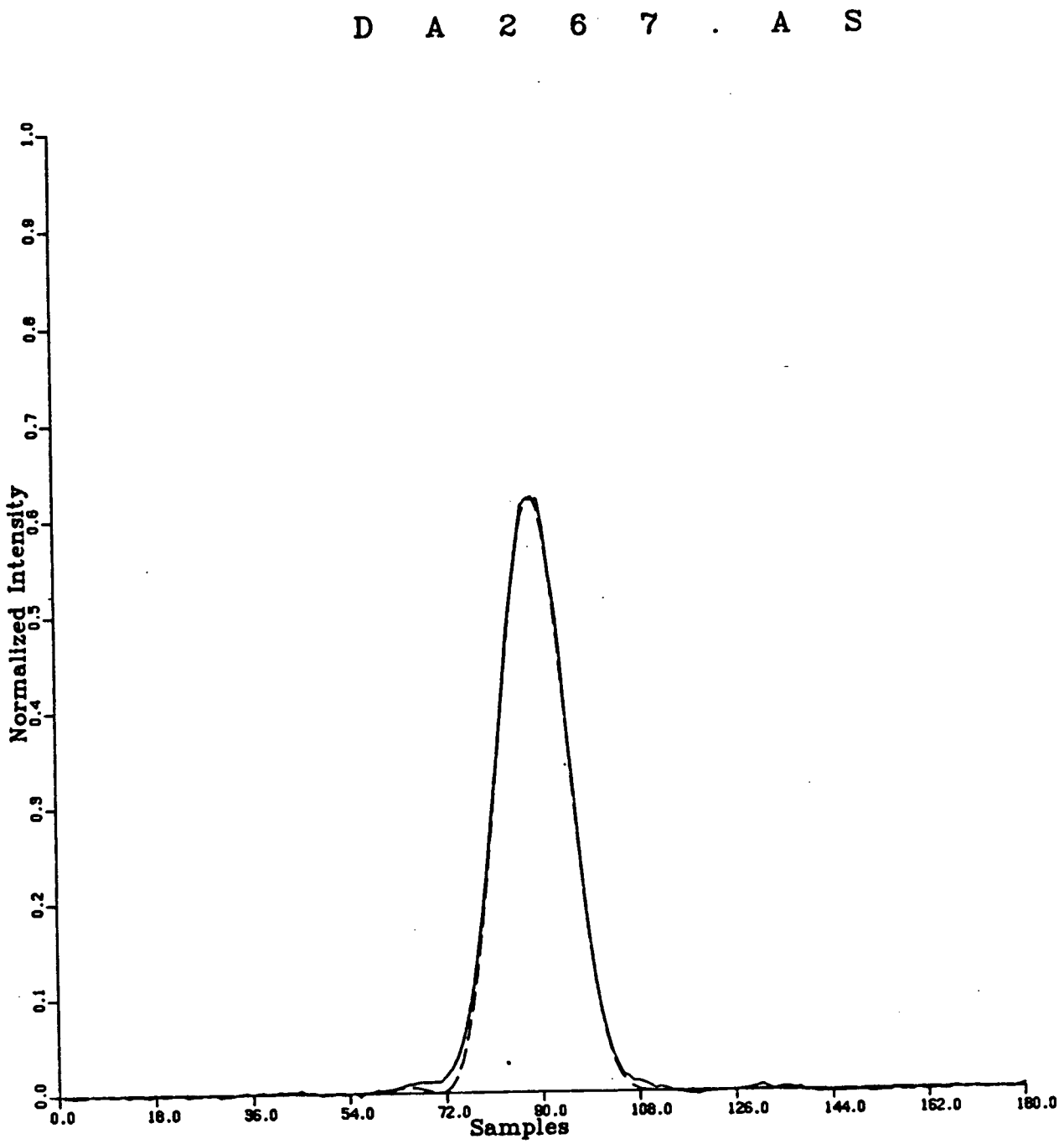

Figure 15. Plot of the final theoretical beam model (dashed lines) superimposed on a 0°-drift scan through the source DA267. The A beam center is 1′ south of the source.

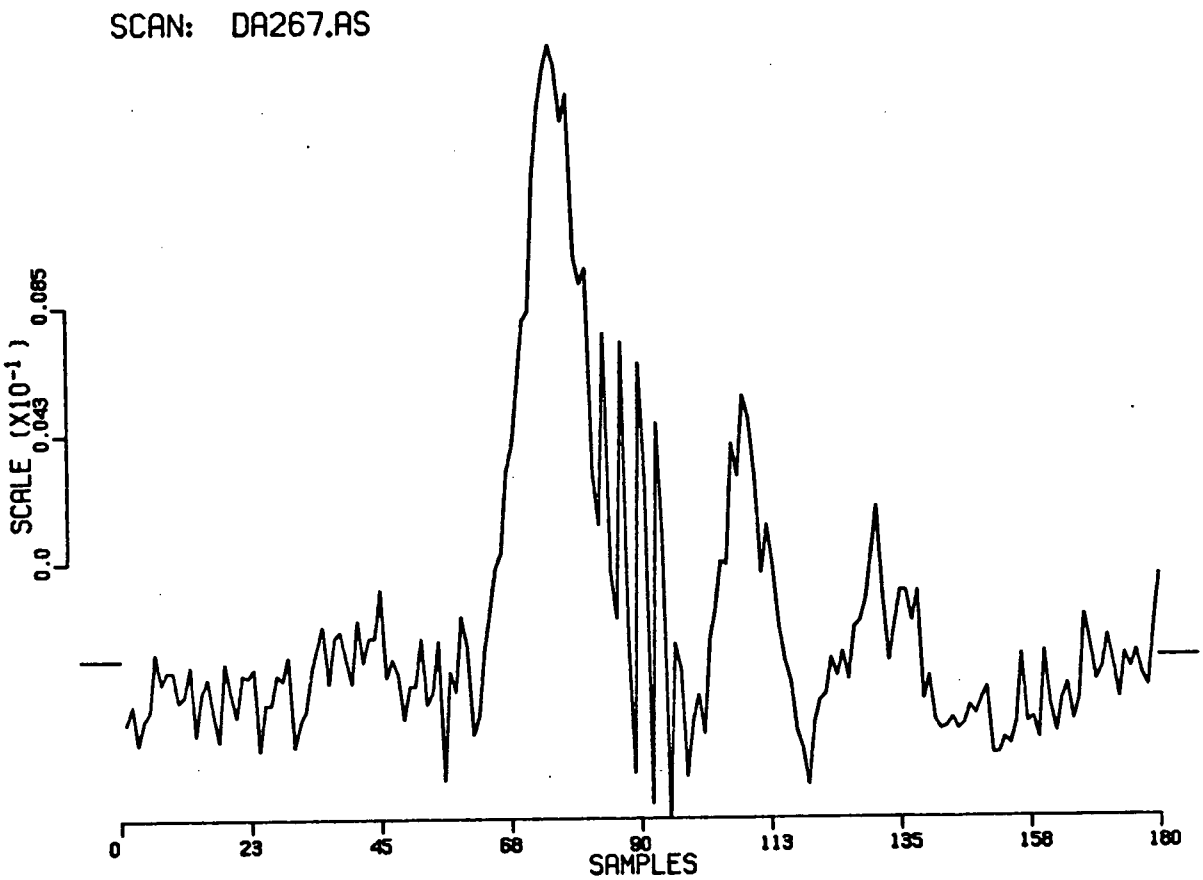

Figure 16. Plot of the residuals between the final theoretical model and the 0°-drift scan through the source DA267. The A beam center is 1′ south of the source. The maximum residual is 1.9% of the beam peak.

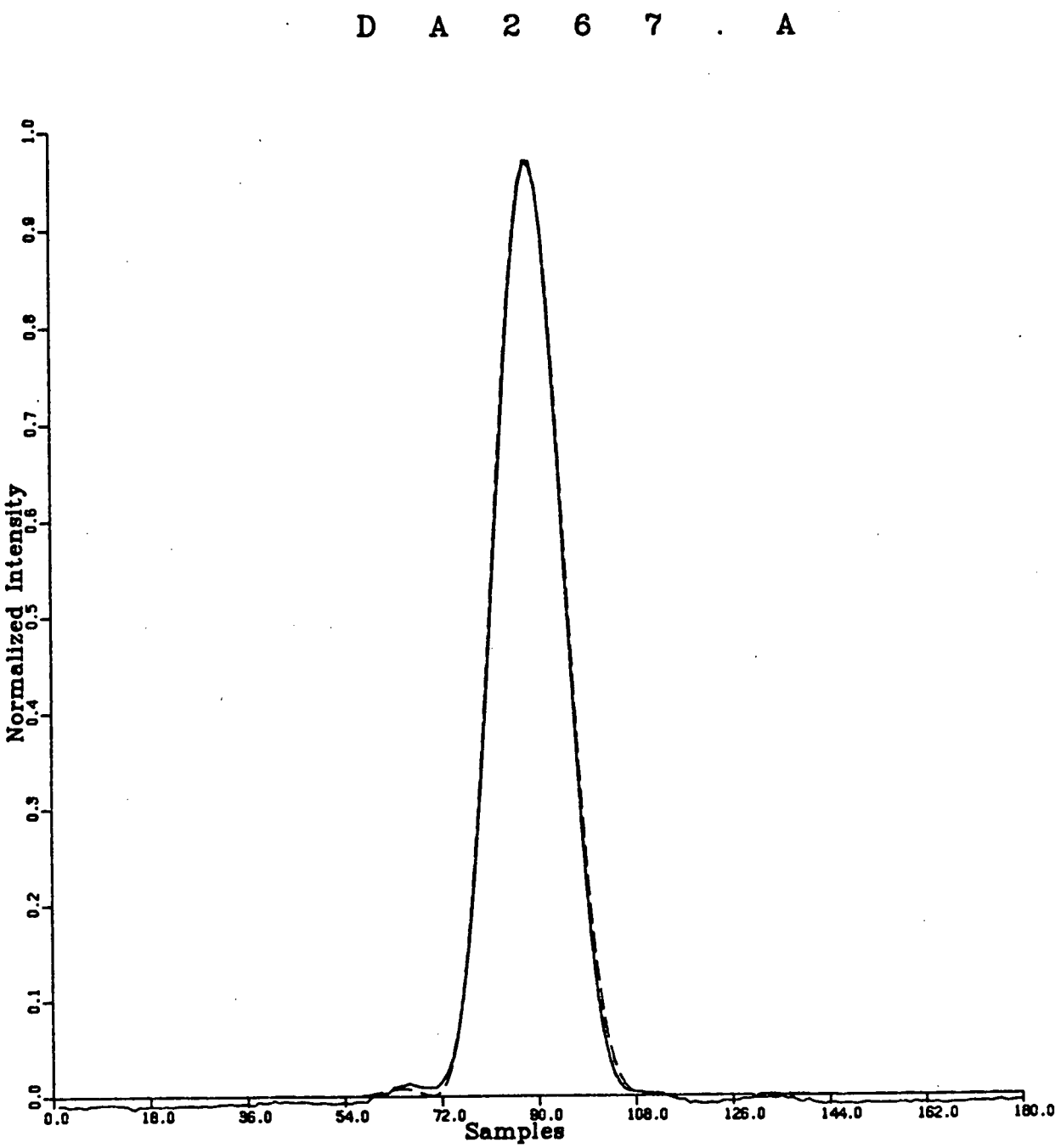

Figure 17. Plot of the final theoretical beam model (dashed lines) superimposed on a 0°-drift scan through source DA267. The A beam center is at the source.

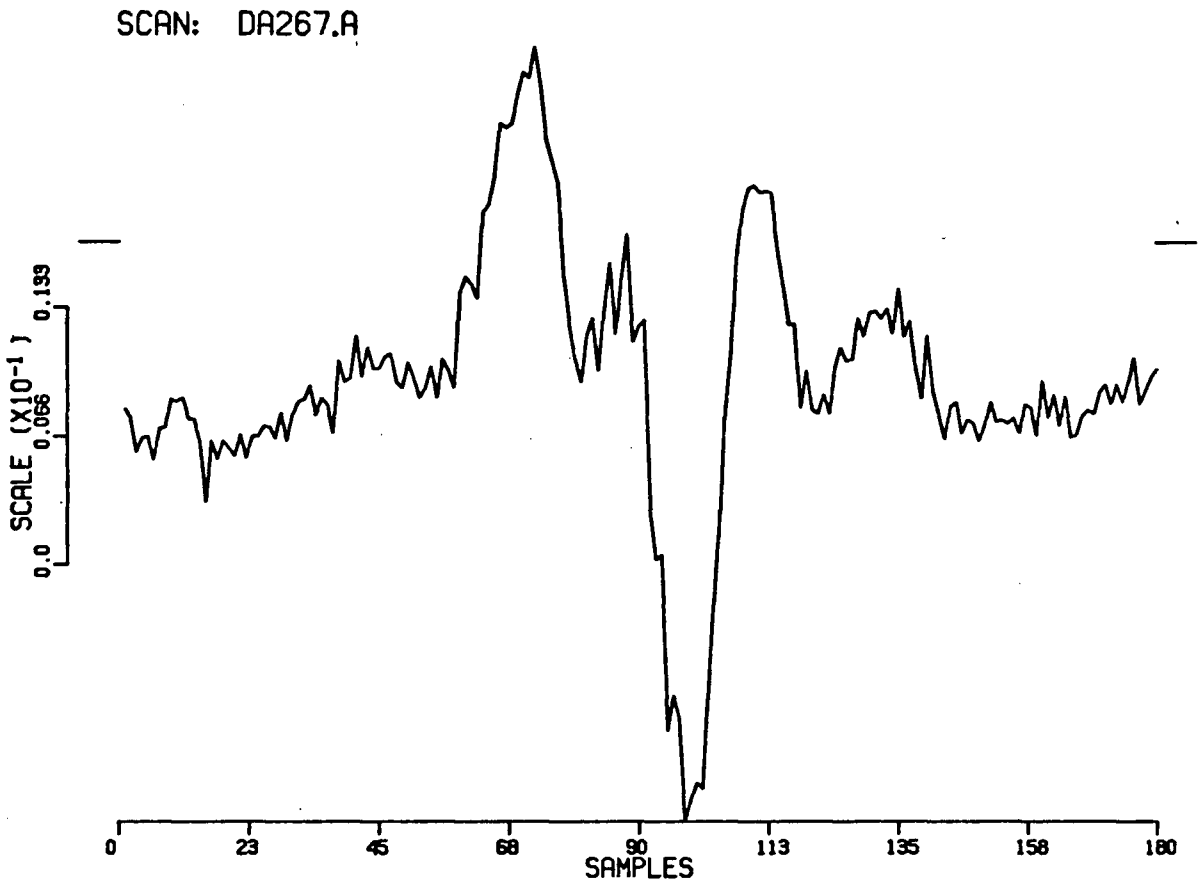

Figure 18. Plot of the residuals between the final theoretical beam model and the 0°-drift scan through the source DA267. The A beam center is at the source. The maximum residual is 2.8% of the beam peak.

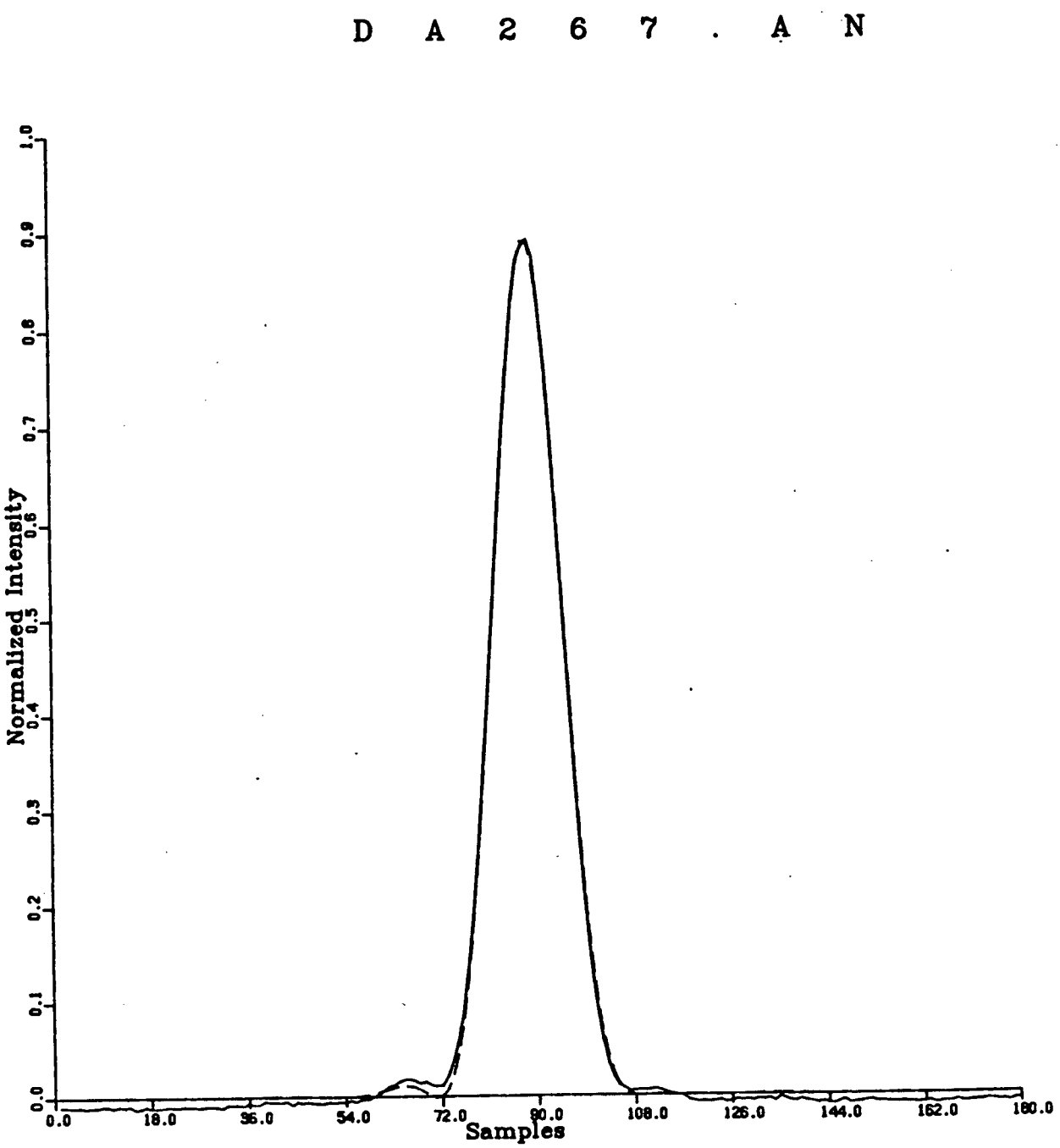

Figure 19. Plot of the final theoretical beam model (dashed lines) superimposed on a 0°-drift scan through source DA267. The A beam center is 1′ north of the source.

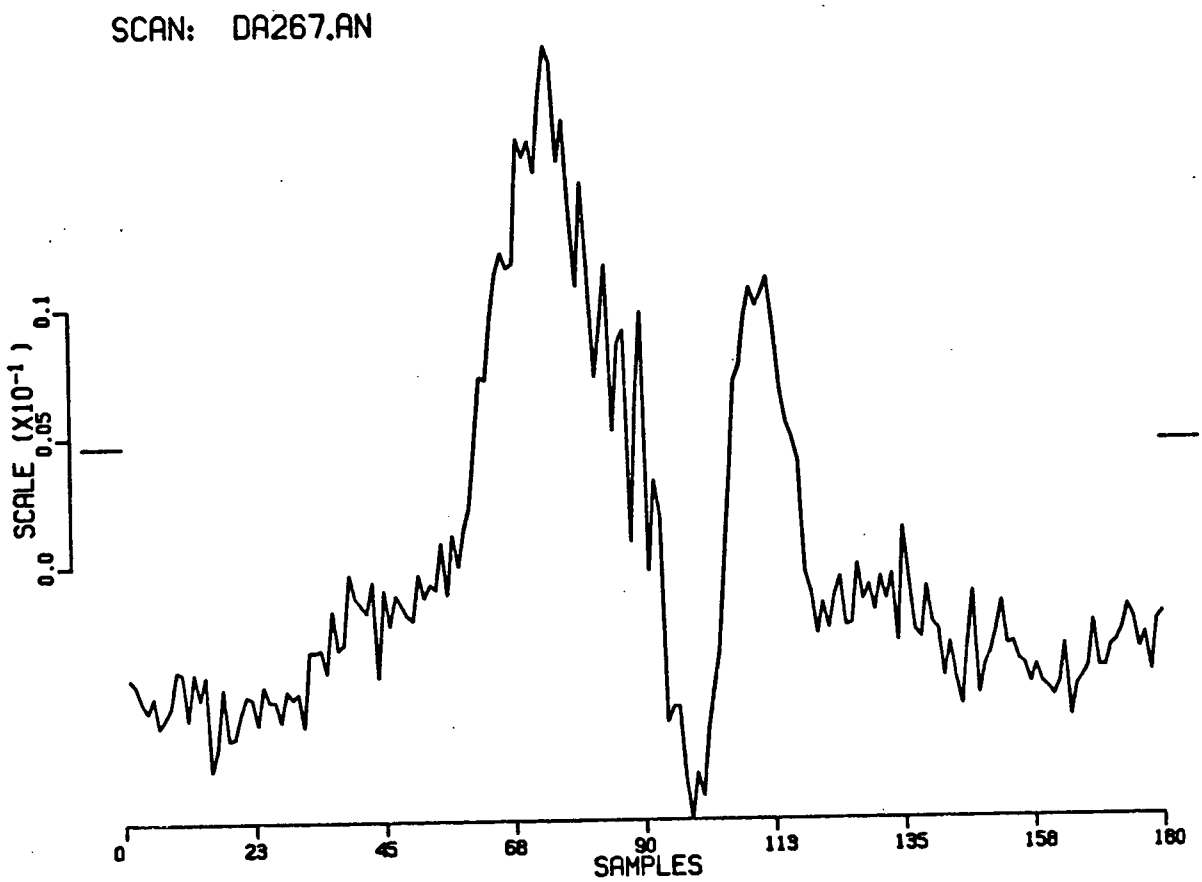

Figure 20. Plot of the residuals between the final theoretical beam model and the 0°-drift scan through the source DA267. The A beam center is 1′ north of the source. The maximum residual is 1.5% of the beam peak.

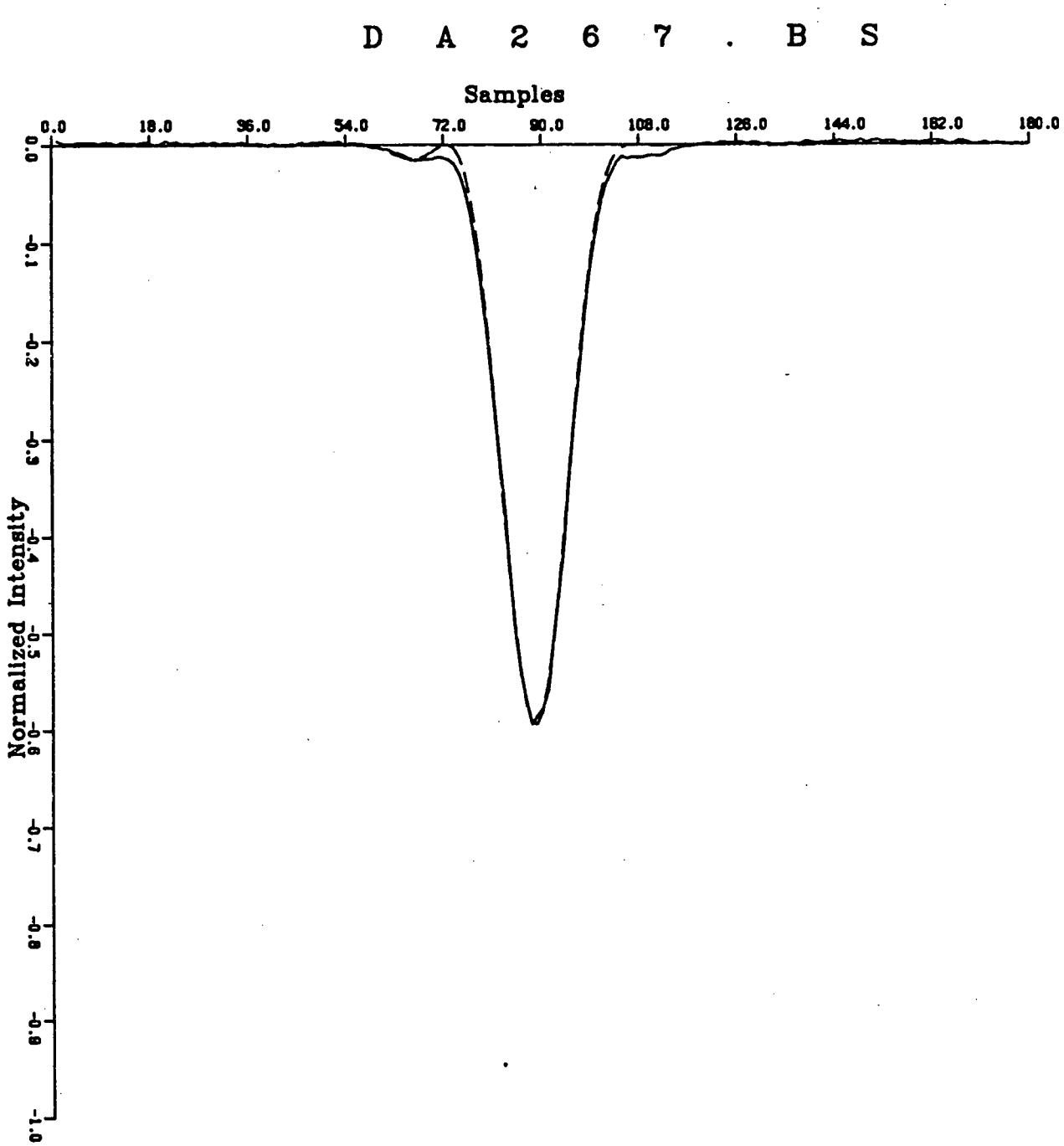

Figure 21. Plot of the final theoretical beam model (dashed lines) superimposed on a 0°-drift scan through the source DA267. The B beam center is 1′ south of the source.

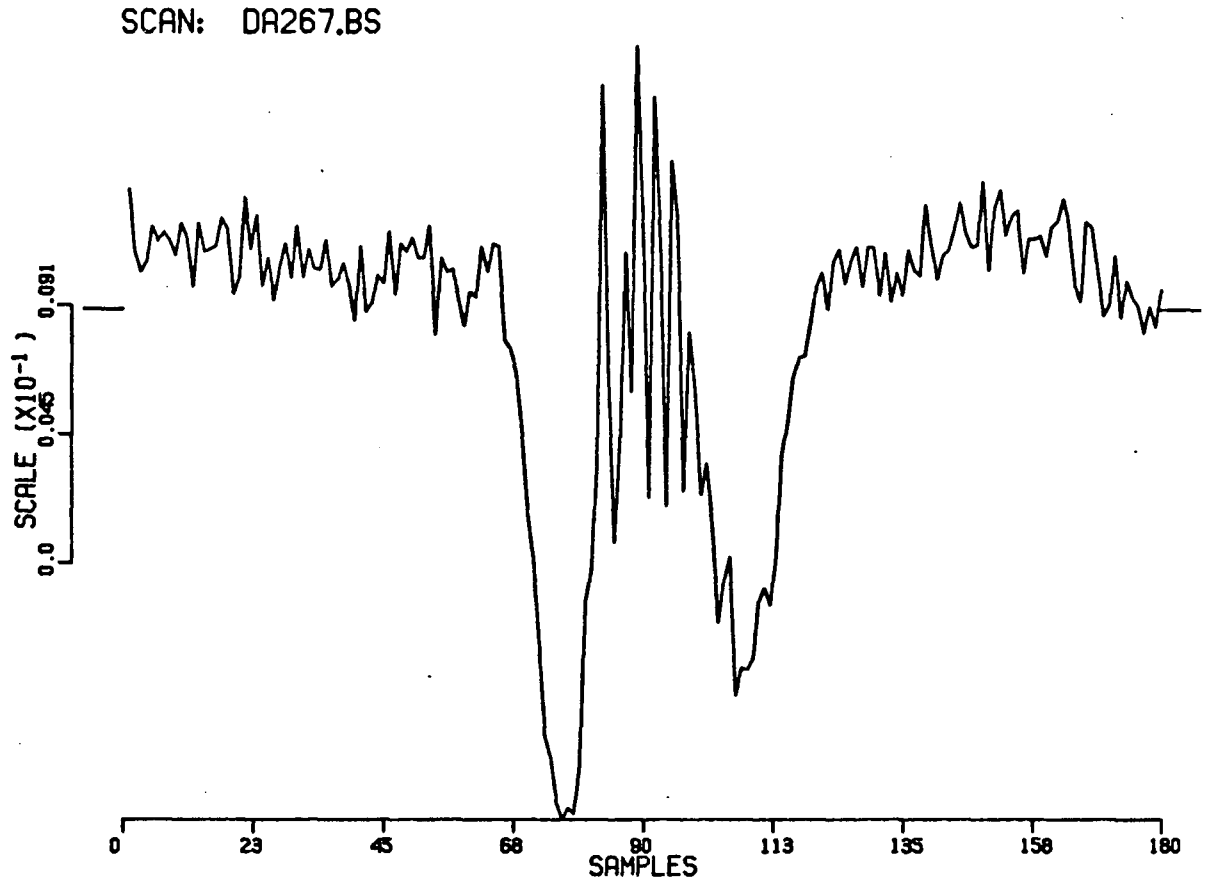

Figure 22. Plot of the residuals between the final theoretical beam model and the 0°-drift scan through the source DA267. The B beam center is 1′ south of the source. The maximum residual is 1.7% of the beam peak.

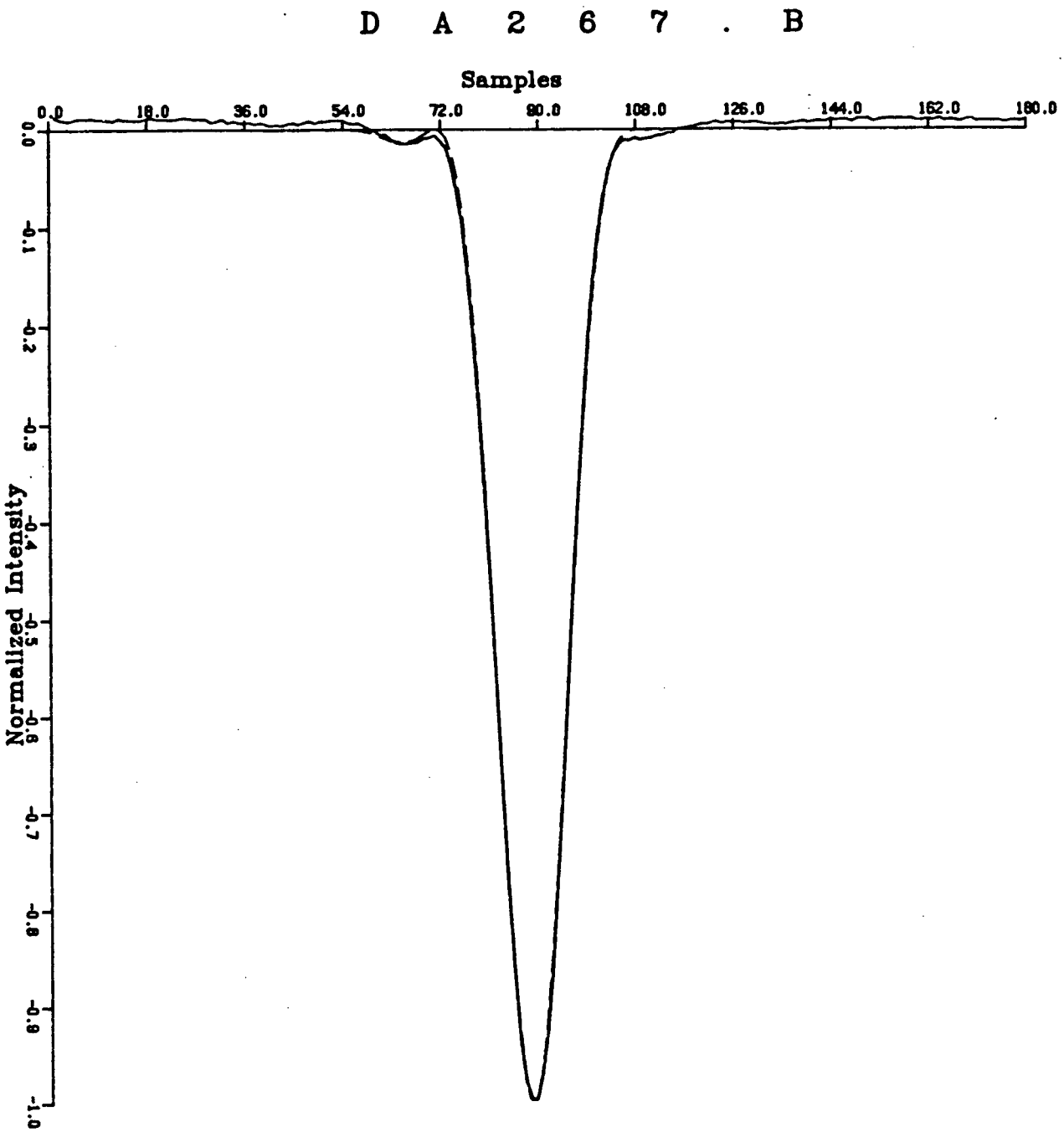

Figure 23. Plot of the final theoretical beam model (dashed lines) superimposed on a 0°-drift scan through the source DA267. The B beam center is at the source.

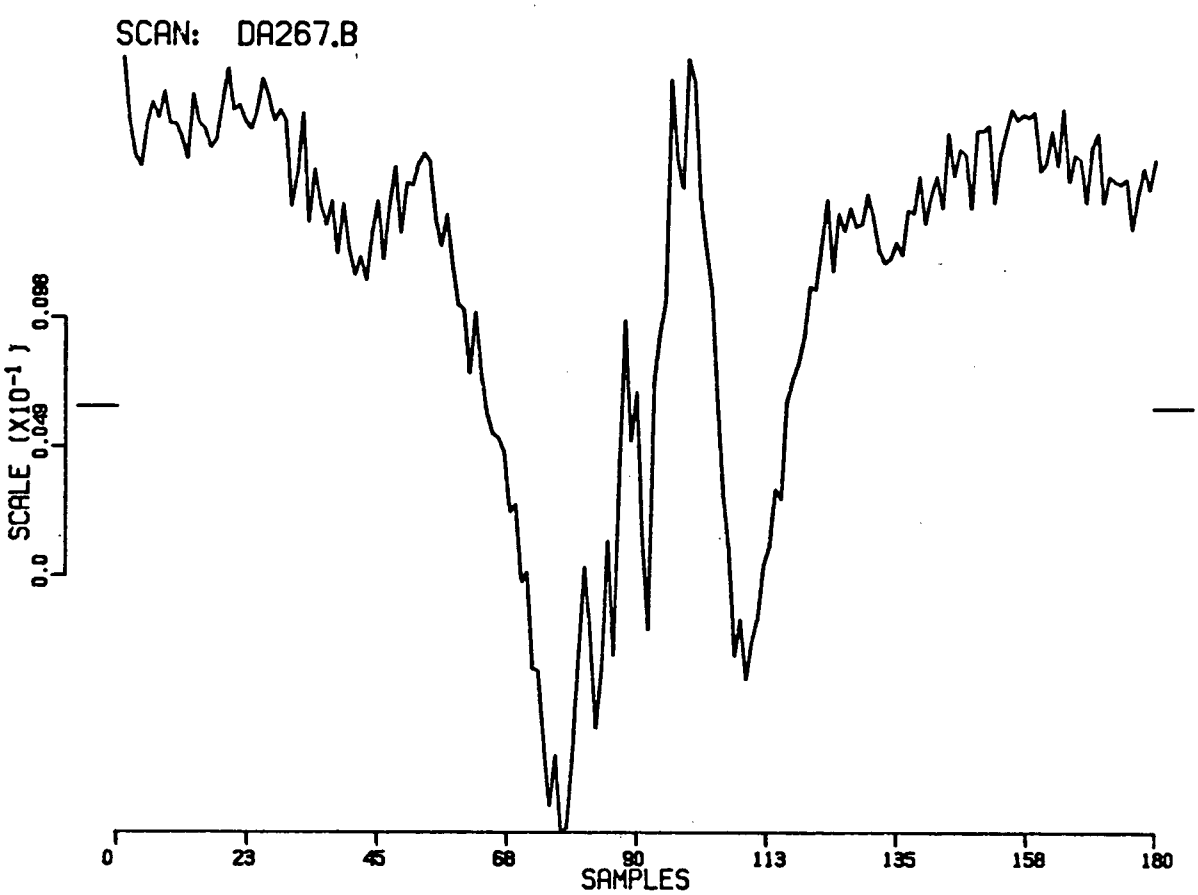

Figure 24. Plot of the residuals between the final theoretical beam model and the 0°-drift scan through the source DA267. The B beam center is at the source. The maximum residual is 1.5% of the beam peak.

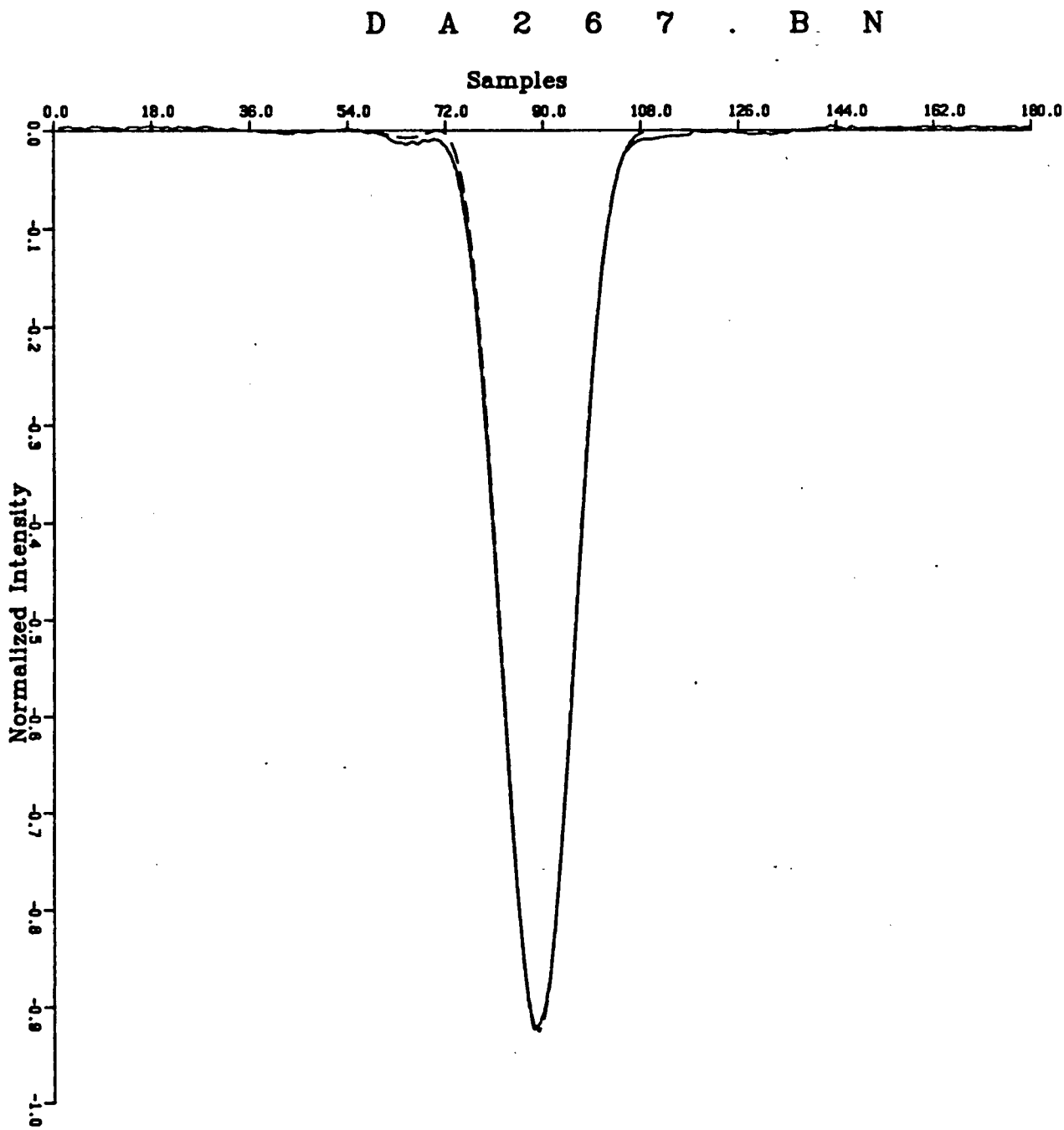

Figure 25. Plot of the final theoretical beam model (dashed lines) superimposed on a 0°-drift scan through the source DA267. The B beam center is 1′ north of the source.

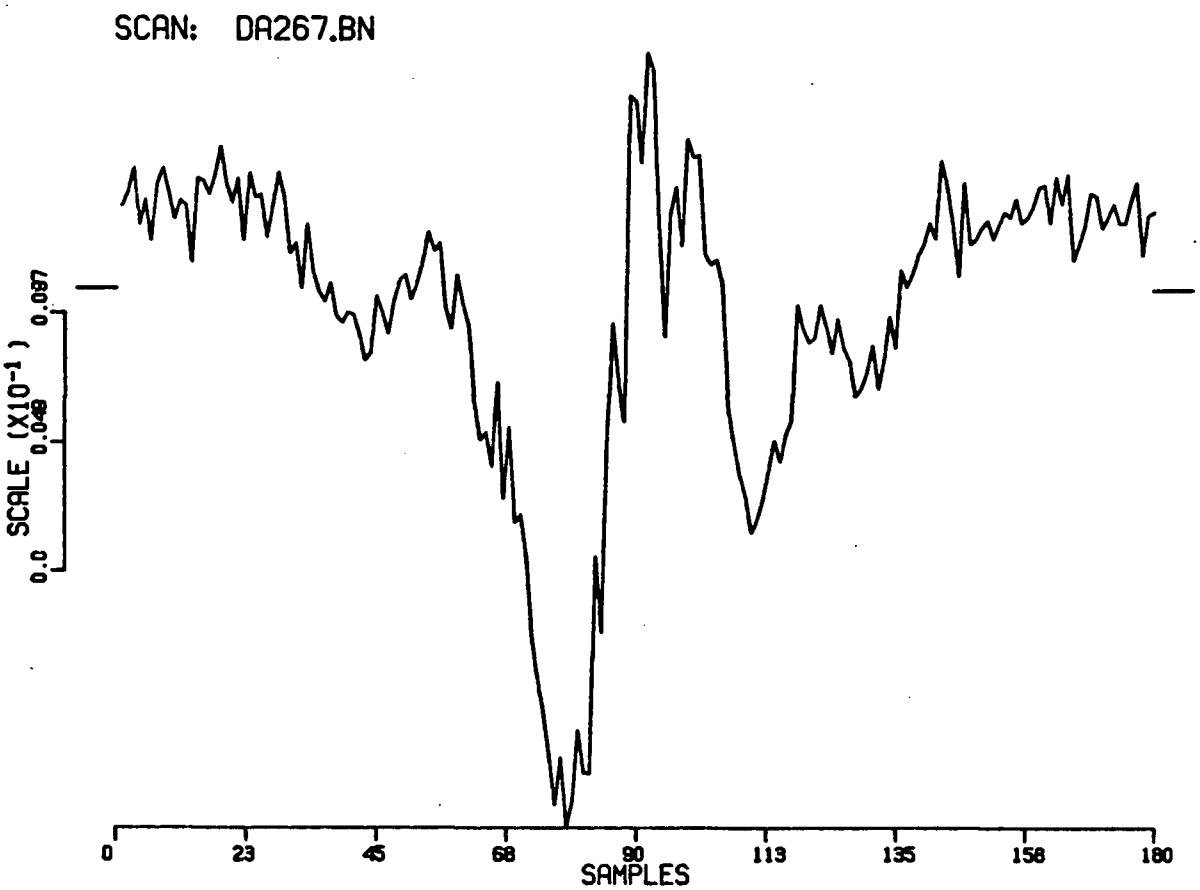

Figure 26. Plot of the residuals between the final theoretical beam model and the 0°-drift scan through the source DA267. The B beam center is 1′ north of the source. The maximum residual is 1.9% of the beam peak.

model to fit the $0° - 60'/min$ driven data. However the residuals of the theoretical model and the observed data are very large (see Figure 28). Further analysis showed that the large residuals are caused by an oscillation in the $0° - 60'/min$ driven data at a frequency of 0.65 Hz(see Appendix B). More importantly, comparison of the $0° - 60'/min$ data with the $11° - 120'/min$ data indicates that the broadening of the telescope beam pattern is dependent on the declination drive rate.

The $11° - 120'/min$ data are the most important data used to calibrate the theoretical model since the Galactic Radio Patrol data base was observed at this drive rate. Each point source observed at $11° - 120'/min$ has three or four repeats of the same scan. The typical $11° - 120'/min$ driven scan has a positive and negative lobe corresponding to feed A and feed B respectively, as does the typical $0° - 60'/min$ scans.

Initially, calibrating the theoretical beam model with the $11° - 120'/min$ data using the same iteration methods as were used for the $0° - 60'/min$ data was not successful since the $11° - 120'/min$ scan peak ratios were all greater than the theoretical beam model peak ratios. This suggested that the scan coordinates were wrong. Furthermore a qualitative analysis of all the $11° - 120'/min$ scans showed that a positive shift in the right ascension coordinate would increase the theoretical beam model peak ratio. Also independent of this work, Dr. N. Duric (personal communication) has found that there is a positive systematic one to two seconds of time difference between point source coordinates derived from observations at the VLA and point source coordinates derived from the Galactic Radio Patrol data base. Consequently to calibrate the theoretical model to the $11° - 120'/min$ driven data, it is necessary to shift the right ascension coordinates until the model and data peak ratios are equal. The iteration method used to determine the shift in the right ascension coordinate was the same as the method used to determine the Δy parameter, with the assumption that the shift in the right ascension coordinate is linearly related to the beam peak ratio. As expected, the theoretical model peak ratio equals the $11° - 120'/min$ data peak ratio when the scan coordinates are shifted

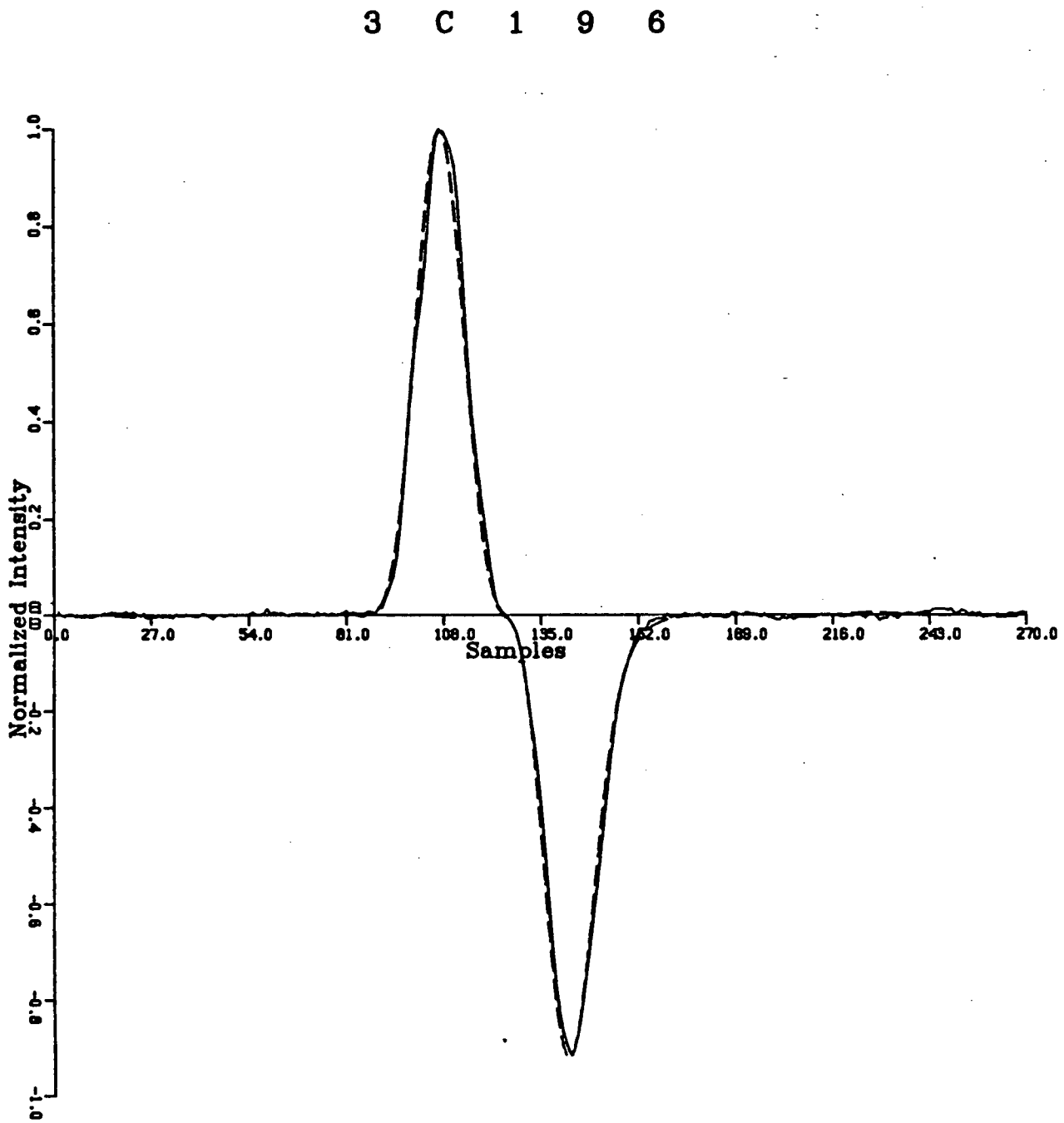

Figure 27. Plot of the final theoretical beam model (dashed lines) superimposed on the $0° - 60'/min$ scan through the source 3C196.

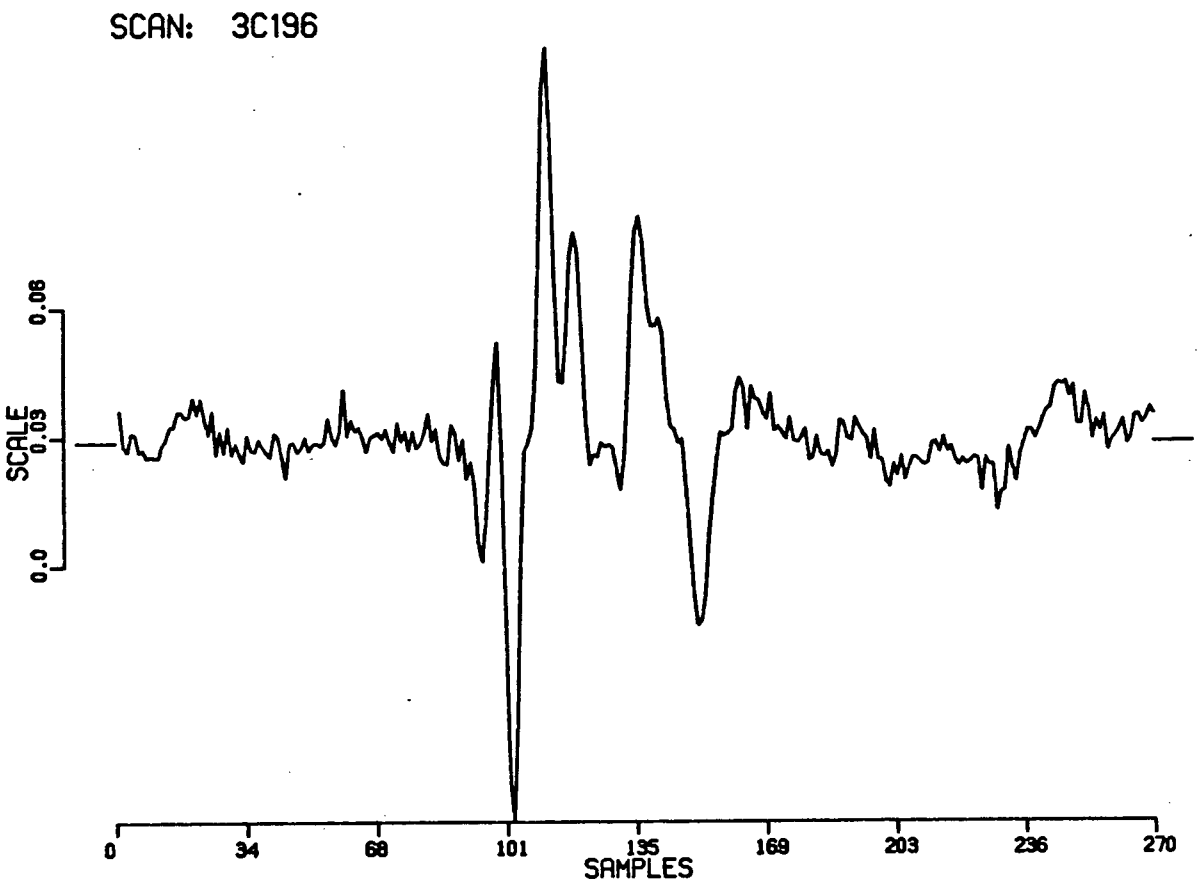

Figure 28. Plot of the residuals between the final theoretical beam model and the $0° - 60'/min$ scan through the source 3C196. The maximum residual is 9.4% of the beam peak.

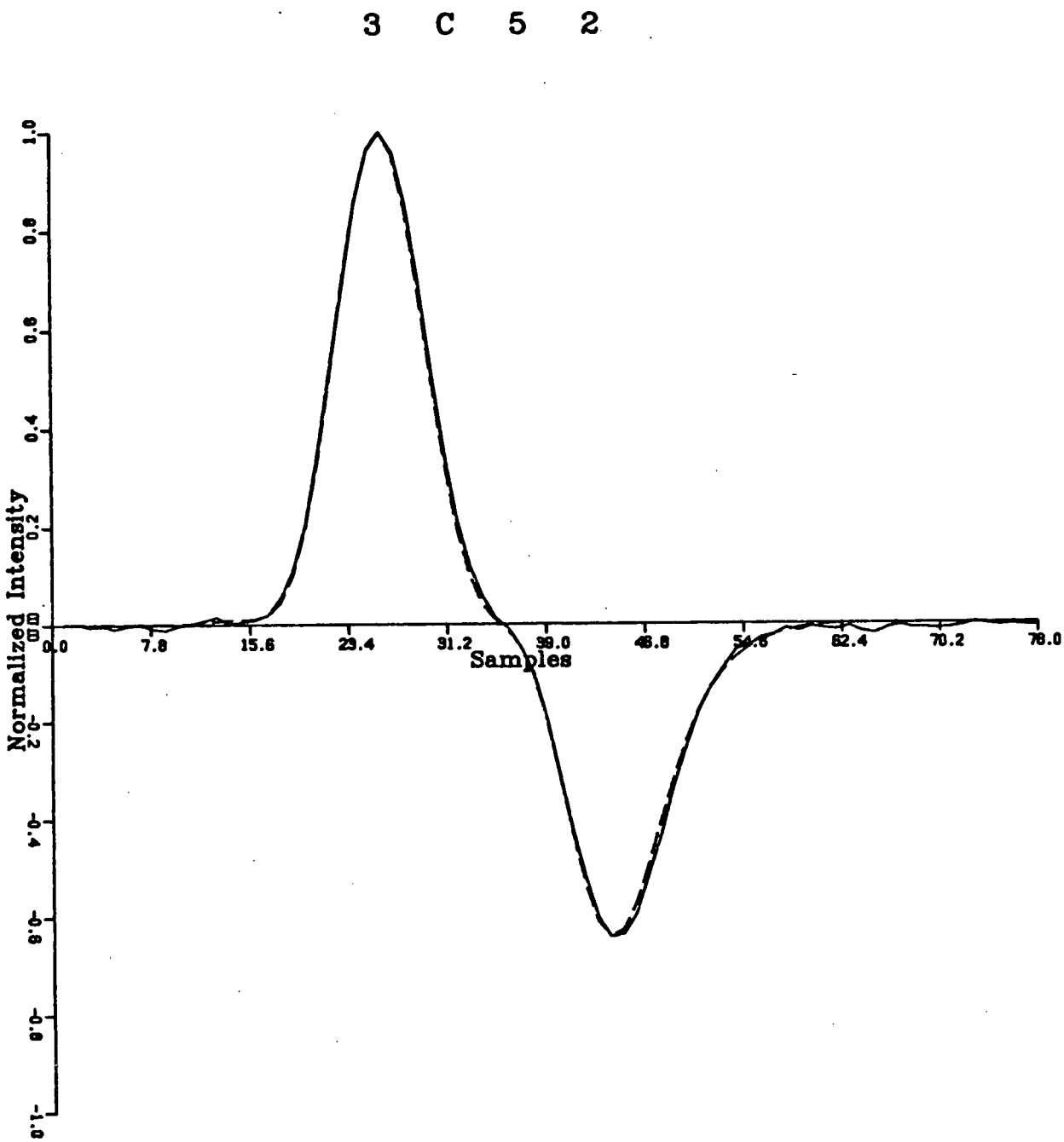

Figure 29. Plot of the final theoretical beam model (dashed lines) superimposed on the $11^\circ - 120'/min$ scan through the source 3C52.

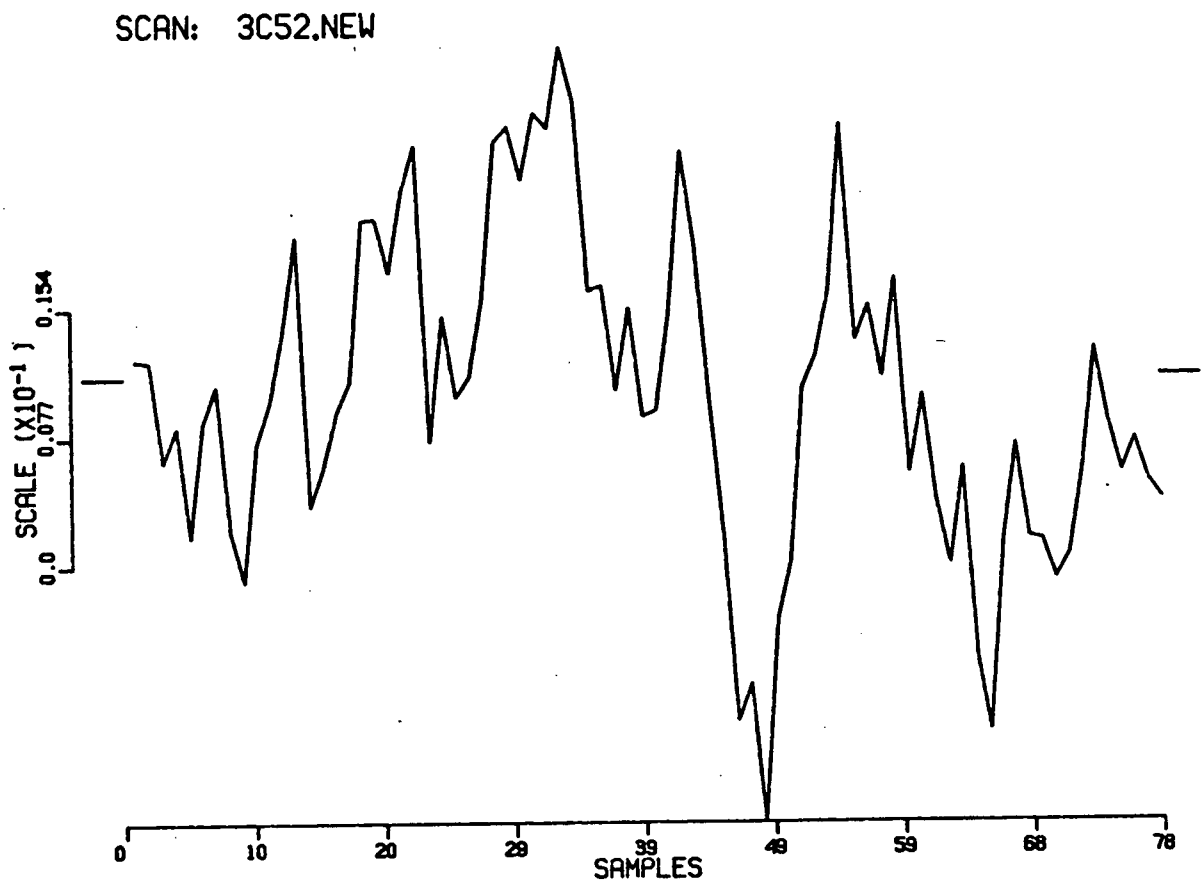

Figure 30. Plot of the residuals between the final theoretical beam model and the $11° - 120'/min$ scan through the source 3C52. The maximum residual is 2.6% of the beam peak.

one to two seconds of time. The EX and H parameters used to calibrate the theoretical model to the $11° - 120'/min$ driven data were determined concurrently. Because the parameters derived for each source are relatively constant, the average parameter values EX =1.03 and $H = 115''$ were used to fit the beam model to the $11° - 120'/min$ driven data. The average peak residual between the theoretical model and the $11° - 120'/min$ data is 3.1%. The final theoretical model fit to the data for the source 3C52 is shown in figure 29 and the residuals are shown in figure 30. Calibration of the theoretical beam model by the $11° - 120'/min$ data shows that there is a positive systematic one to two seconds of time scan coordinate error in the Galactic Radio Patrol data base, and that the observed telescope beam pattern depends on the declination drive rate.

Calibration of the theoretical model by the point source observations, between $23° \leq \delta \leq 62°$ added three more parameters to the theoretical model. The y axis shift parameter was constrained by the 90° drift scans to be -0.022 meters. The feed separation parameter EX and the gaussian half power width parameter H were found to depend on the declination drive rate. Table II summarizes the Δy, EX, and H parameter values for the 90°-drift, 0°-drift, $0° - 60'/min$, and $11° - 120'/min$ data scans. The broadening of the beam between the 90°-drift data and the $0° - 60'/min$ driven data was thought possibly to be a daytime versus nighttime effect. This idea is contradicted by the fact that both the 90°-drift scans and the $0° - 60'/min$ scans were observed during the daytime. Unfortunately there are no driven scans which would illustrate the declination driven telescope beam pattern perpendicular to the scan direction. Several parallel driven scans, offset one to two arcminutes, must be used to determine the telescope beam perpendicular to the scan direction, since at the high declination drive rates of $60'/min$ and $120'/min$ the scan direction is within 14° and 7° of the telescope meridian. Instead it was assumed that there was no declination drive rate broadening in the right ascension direction. The good fit of the model to the 0°-drift scans after the model was calibrated by the 90° -drift scans is consistent with this assumption. The addition of the y shift

parameter Δy, the feed separation factor EX, and the gaussian half power beam width parameter H to the theoretical beam model enabled the beam model to be calibrated by the data observed at the three different declination drive rates.

Table II.

Summary of the Theoretical Beam Model Parameters

Scan Type	Δy (meters)	EX	H (arcseconds)	Average Peak Residual	# Sources Observed
90°-drift	$-.022 \pm .003$	$1.01 \pm .005$		3.7%	9
0°-drift	$-.022 \pm .003$	$1.01 \pm .005$		2.8%	10
$0° - 60'/min$	$-.022 \pm .003$	$1.01 \pm .005$	89 ± 8	7.1%	8
$11° - 120'/min$	$-.022 \pm .003$	$1.03 \pm .005$	115 ± 6	3.1%	4

VI. Comparison with Previous Beam Model

Now that the theoretical beam model has been calibrated it is possible to compare its performance to that of the older empirical beam model (Braun 1981). The objective is to choose the beam model which best represents the actual beam. Since the calibration work shows that the beam pattern is dependent on the telescope drive rate, and the Galactic Radio Patrol data are $120'/min$ declination driven scans, the only useful data to evaluate the two beam models are the $120'/min$ driven data. With this in mind two separate methods were used to evaluate the beam models. One method derived from the calibration work finds the average peak residual between the beam models and the $120'/min$ driven scans. The second method compares two separate full intensity sky maps generated using the two beams, a section of the Galactic Radio Patrol data base, and a maximum entropy deconvolution algorithm. An estimate of each beam model's dynamic range was made using these two comparison methods.

Throughout this comparison the parameters used by the theoretical model are $\Delta y = -0.022$ meters, $EX = 1.03$ and $H = 115''$ (see Figure 31). The older empirical beam model above 10% of its peak is a modified gaussian whose parameters are determined from 0°-drift scans and $0° - 60'/min$ scans. A gaussian is fitted to the empirical beam model below the 10% peak level (see Figure 32).

The same methods were used to compare scans as were used in the calibration process. Both beam models were shifted one to two seconds of time in right ascension until the model peak ratios equaled the observed data peak ratios. As mentioned earlier, there is only one scan track through each source. For all four sources the theoretical model fits the data much better than the empirical model (see Figures 29, 30, 33, and 34). The average peak residual of the theoretical model is 3.1%, and the average peak residual of the empirical model is 10.6%. Thus the theoretical beam model should have a dynamic range of 32:1 whereas the empirical beam model should have a dynamic range of only

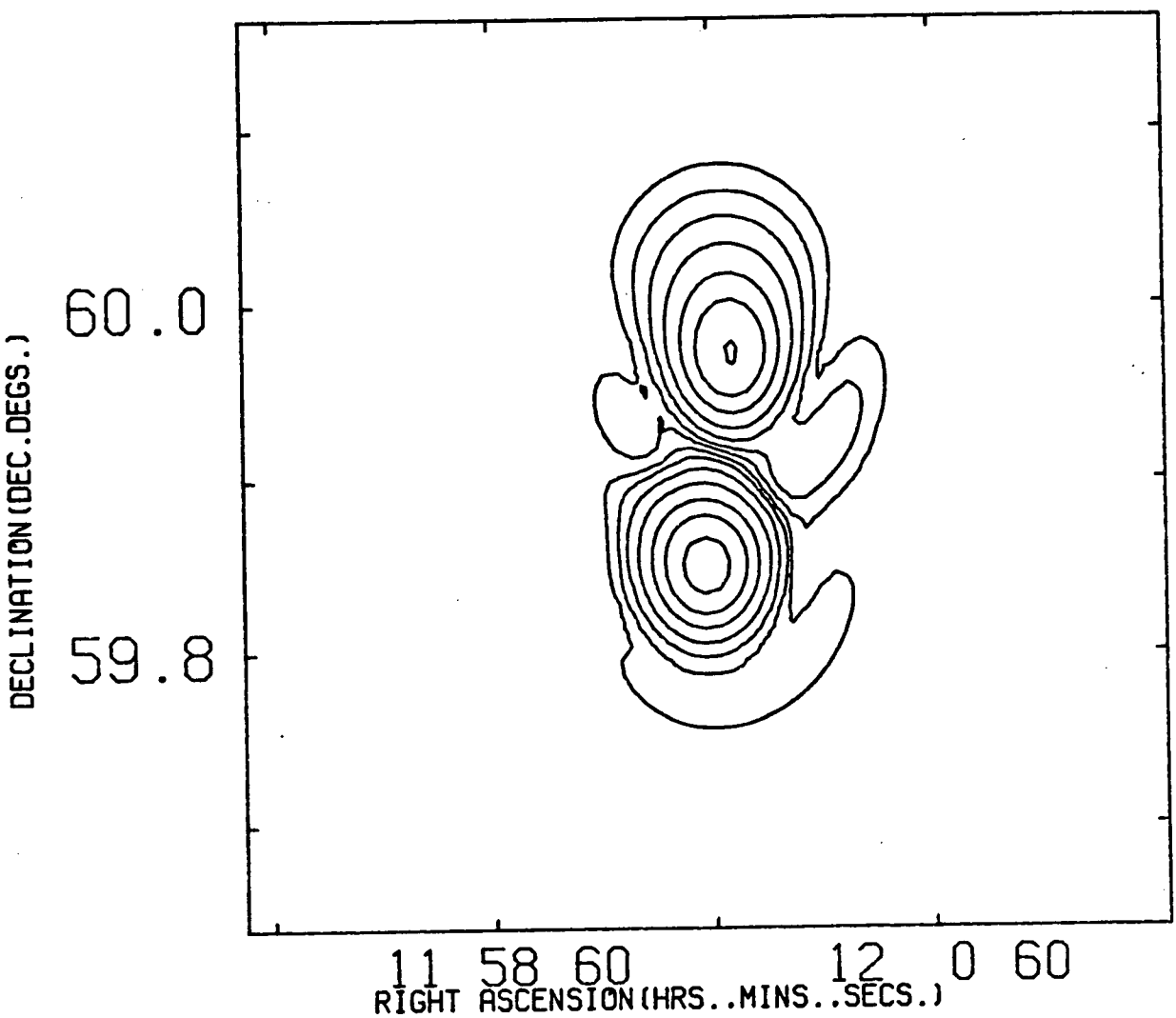

Figure 31. Contour map of the theoretical beam model for a declination of 59.9°. The contour values are ± 80, 50, 30, 15, 7, 3, and 1% of the beam peak.

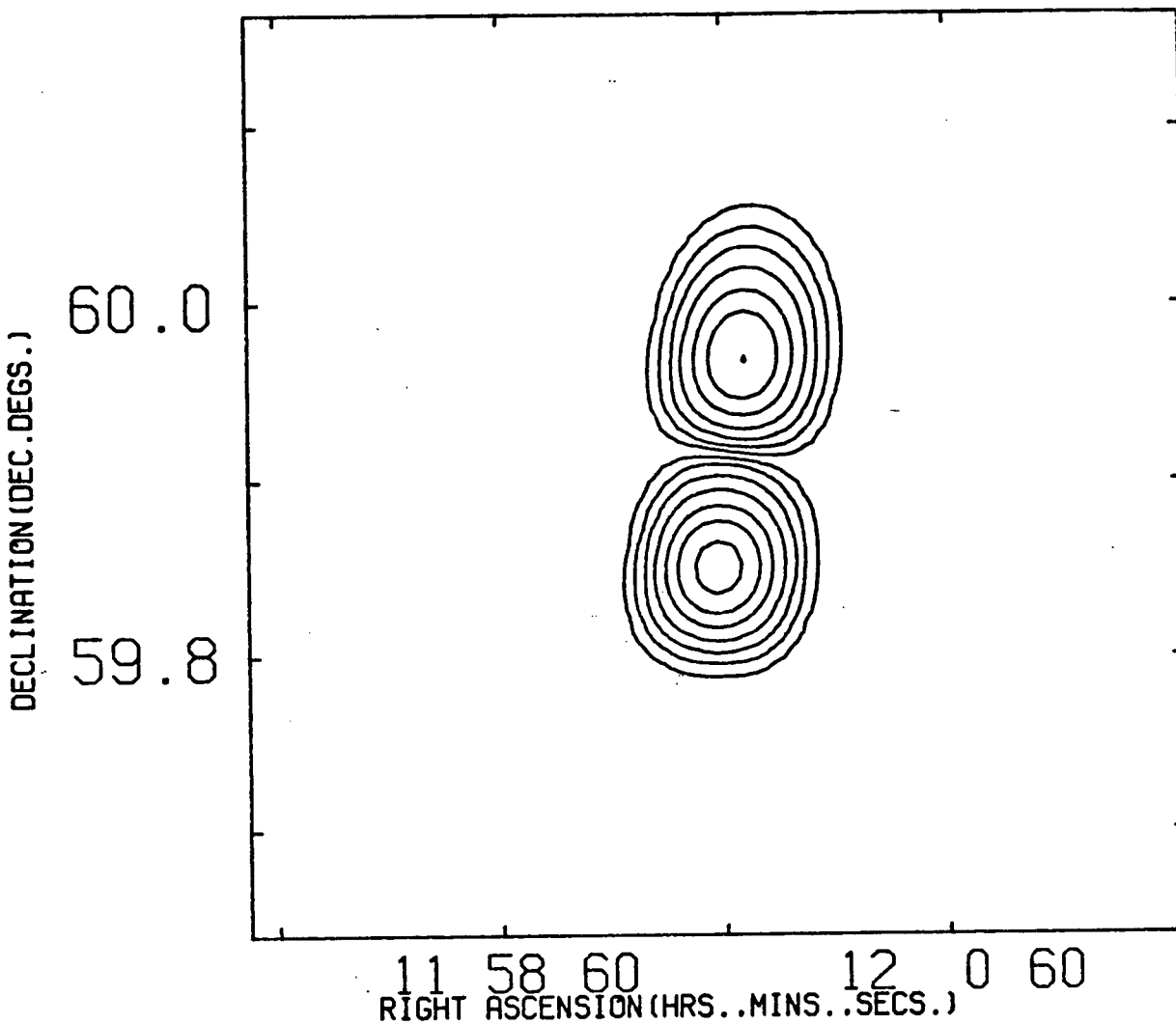

Figure 32. Contour map of the previous empirical beam model for a declination of 59.9°. The contour values are ± 80, 50, 30, 15, 7, 3, and 1% of the beam peak.

10:1. Consequently the $11° - 120'/min$ data show the theoretical beam to be 3 times more accurate than the empirical beam model.

The second method used to evaluate the accuracy of the beam models is to deconvolve the differential beam from a small area of the Galactic Radio Patrol data base. The area of sky was chosen so that it had both extended structure and an unresolved point structure. The region of sky from $\alpha = 23^h\,12^m\,15^s$ to $\alpha = 23^h\,19^m\,0^s$ and from $\delta = 58.8°$ to $\delta = 61.0°$ contains Sharpless objects 157 and 156. S157 has extended structure surrounding it, and S156 is a compact H II region. The $11° - 120'/min$ scan data of this region were placed in a 256x256 point grid with the space between grid points being $0.5'$ (Braun 1981). Next a maximum entropy deconvolution method (Gull *et al* 1978) using the theoretical beam model and the empirical beam model produced two full intensity sky maps of the area (using the software of Braun 1981). The noise and default level parameters were set to 18 mK and 15 mK respectively. After 40 iterations the map generated using the theoretical beam model (new beam map) converged with $\chi^2 = 1.25707$, and the map generated using the empirical beam model (old beam map) converged with $\chi^2 = 1.13413$ (see Figures 35 and 36). Generally the two maps have the same structure; however, detailed analysis shows that all the peak values of the new beam map are greater than the peak values of the old beam map. Furthermore the unresolved sources on the new map are more circular than the unresolved sources on the old beam map. In fact the empirical beam model seems to produce triangular shaped point sources.

The compact H II region S156 was used to determine the dynamic range of each beam. From the high resolution observations done by F. P. Israel (1977) S156 is shown to be a relatively isolated radio source with an angular extent of approximately $15''$. Since the telescope beam has an angular extent of approximately $3'$, S156 is essentially a point source compared to the NRAO 91 meter telescope beam. With the assumption that the small sources surrounding S156 are artifacts of the beam, the ratio of the S156

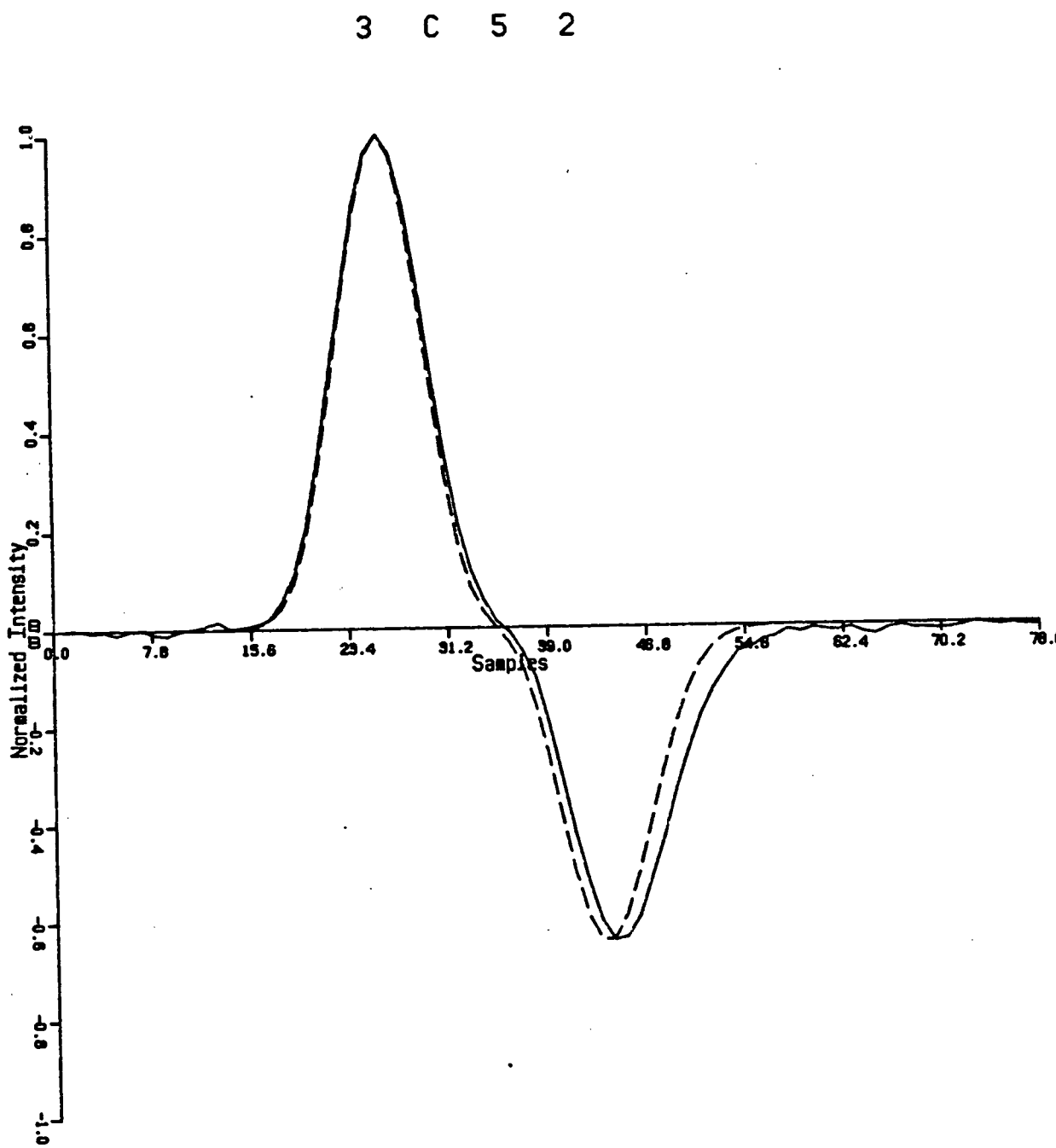

Figure 33. Plot of the previous empirical beam model (dashed lines) superimposed on the $11° - 120'/min$ scan through the source 3C52.

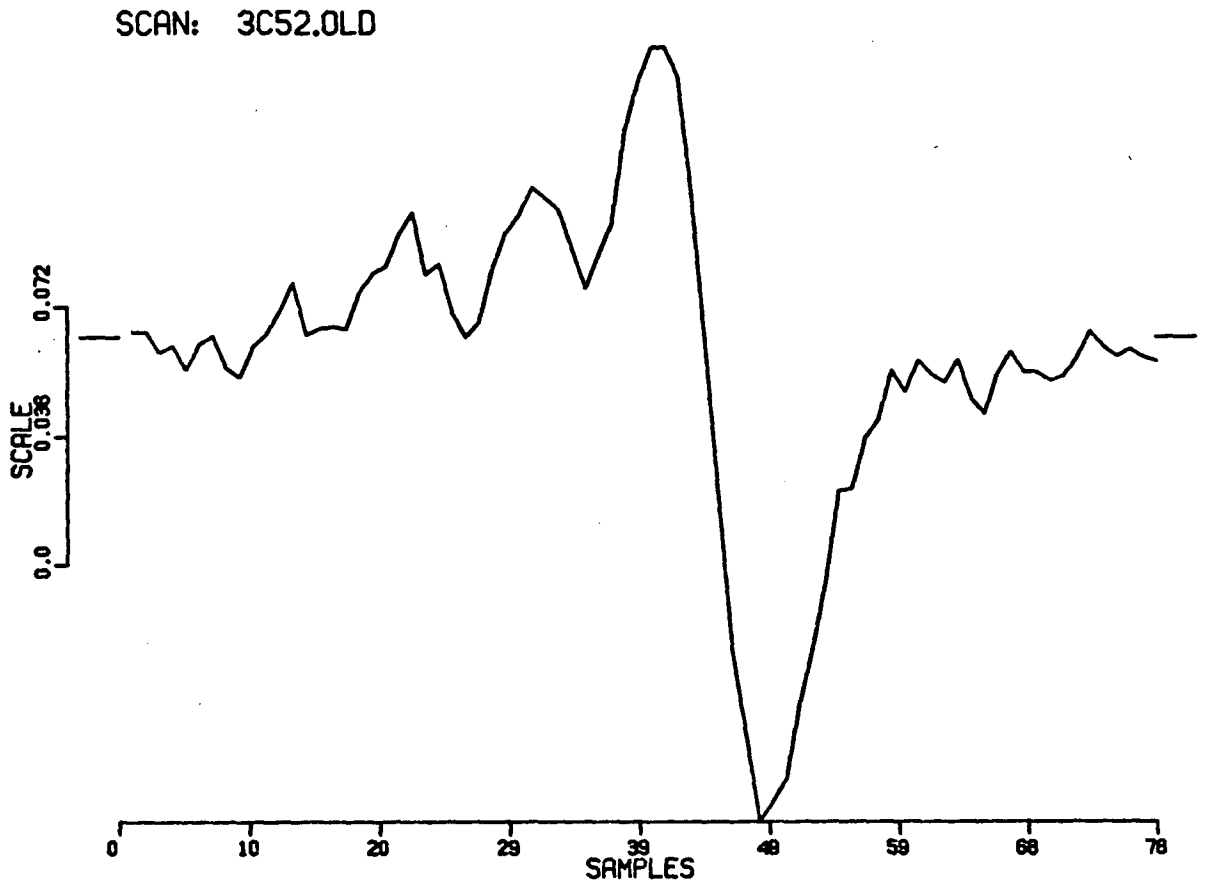

Figure 34. Plot of the residuals between the previous empirical beam model and the $11° - 120'/min$ scan through the source 3C52. The maximum residual is 13.4% of the beam peak.

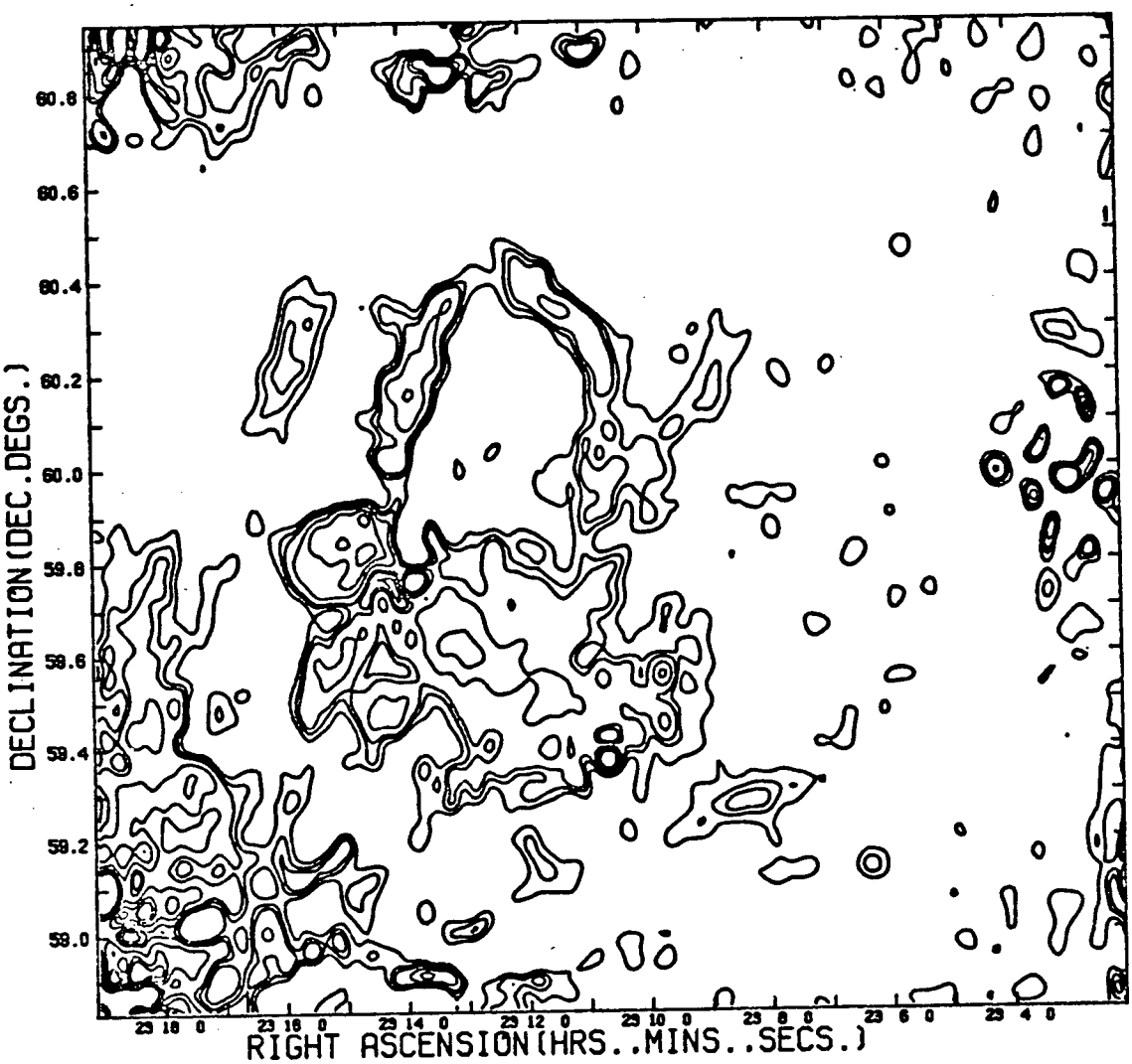

Figure 35. Contour map of the test area deconvolved with the theoretical beam model. Contour values are 500, 300, 150, 70, 50, and 30 mK.

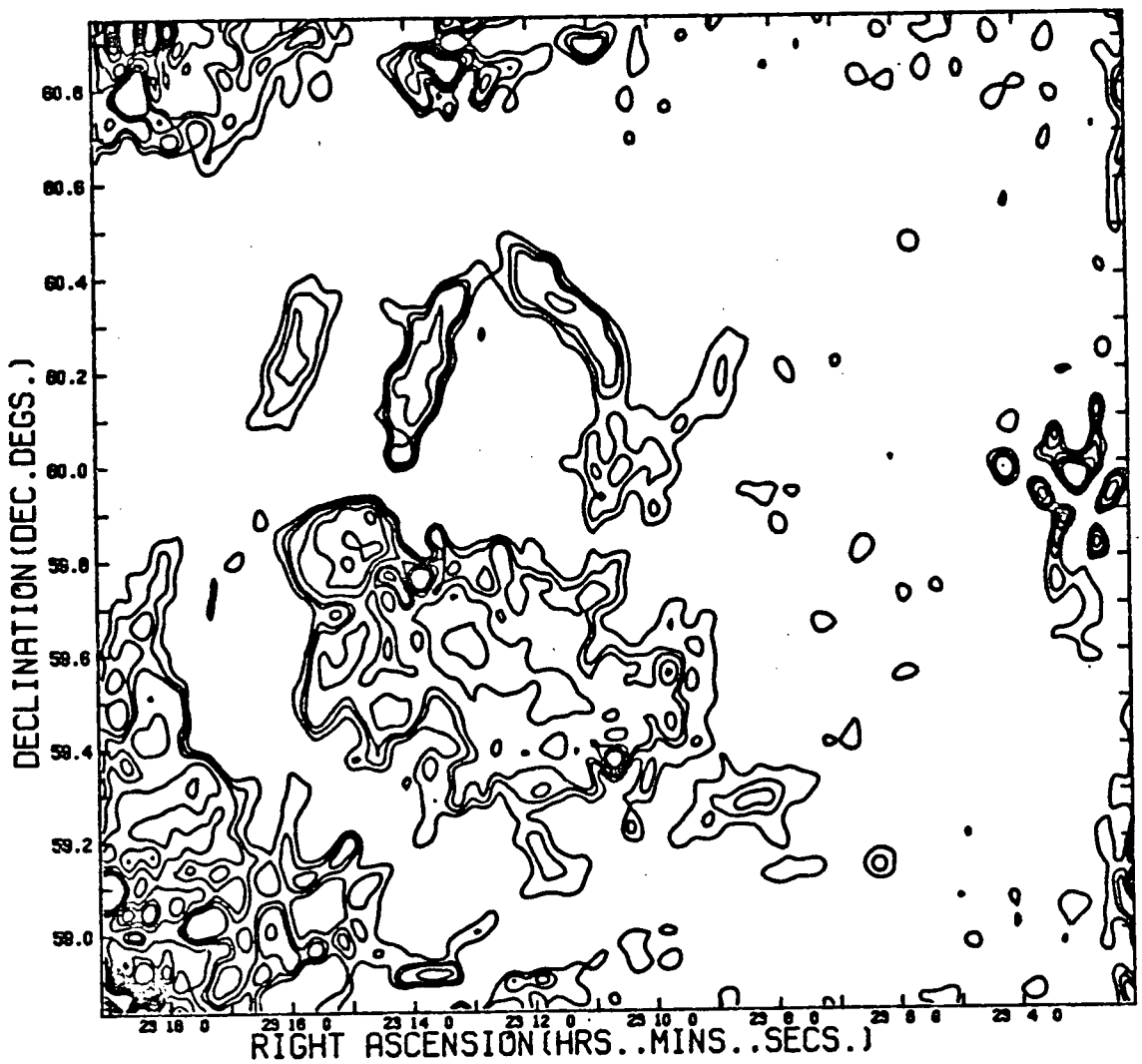

Figure 36. Contour map of the test area deconvolved with the empirical beam model. Contour values are 500, 300, 150, 70, 50, and 30 mK.

peak value to the peak artifact value gives an estimate of the dynamic range of each beam model. On the new beam map the peak value of S156 is 11,130 mK, and the peak value of the sources surrounding S156 is 372 mK; and on the old beam map the peak value of S156 is 7,561 mK, and the peak value of the sources surrounding S156 is 443 mK. Thus the new beam map shows that the theoretical beam model has a dynamic range of 30:1 whereas the old beam map shows that the empirical beam model has a dynamic range of much less than 17:1 since the triangular shaped point sources are not believable.

Both the single scan data and the maximum entropy method full-intensity maps show that the theoretical beam model is more accurate than the empirical beam model.

VII. Conclusions

Two major results have come from this work: a theoretical beam model has been developed accurate to 3% of the peak to describe the NRAO 91 meter telescope beam at 6 cm; and new instrumental effects of the NRAO 91 meter telescope have been observed and discussed.

The main achievement of this work was the development of the theoretical beam model which, compared with the previous empirical beam model, was shown in two separate tests to be more useful. A comparison of the models for $120'/min$ declination driven scans shows that the theoretical model is accurate to 3% of the beam peak (for $23° \leq \delta \leq 62°$), whereas the empirical model is accurate to only 10% of the beam peak. Furthermore, a full intensity map generated from the data by a maximum entropy deconvolution method and the theoretical beam model achieved a dynamic range of approximately 30:1. It is expected that the theoretical beam model developed in this work will greatly simplify the calibration of the new seven feed receiver planned for the NRAO 91 meter telescope.

Three new instrumental effects of the NRAO 91 meter telescope were discovered: the beam shape broadening, the oscillations in the $0° - 60'/min$ data, and the beam peak point separation. The beam shape broadening was modeled by the convolution of a one-dimensional declination direction gaussian of half power beam width H with the theoretical model. For the drift, $60'/min$ and $120'/min$ scans H equaled $0''$, $89''$, and $115''$ respectively. The cause of beam broadening is not understood, but high frequency oscillations are the suspected cause. The residuals of $0°$-$60'/min$ data and the theoretical model showed that there is an oscillation of 0.65 Hz in the data. This oscillation increases the noise in the data to approximately 10% of the scan peak. Fortunately oscillations were not observed in the drift or $120'/min$ declination driven scans. The comparison of the theoretical model to the observed data showed that the beam peak point separation

depends on the declination drive rate, as both the drift and $60'/min$ scans had a feed separation factor of 1.01, and the $120'/min$ scans had a feed separation factor of 1.03. All these results indicate that work should be done to improve the declination drive mechanism of the NRAO 91 meter telescope; however, while the instrumental effects of the telescope persist, $60'/min$ drive rate scans should not be used for observations requiring high dynamic range mapping, and scans at different drive rates should not be compared directly.

References

Abramowitz, M., and Stegun, I.A. (Eds.).(1972). *Handbook of Mathematical Functions.* New York: Dover.

Braun, Robert. (1981). *Radio Continuum Observations of the Supernova Remnant G109.1-1.0.* Unpublished master's thesis, University of British Columbia, Vancouver, B. C.

Fisher, J.R., and Payne, H.E.(1982). *Measurements of the North-South Focal Point Motion and Astigmatism of the 300 Foot Telescope.* Engineering Memo No.148, NRAO Green Bank, West Virginia.

Gregory, P.C., and Taylor, A.R.(1981). "Radio Patrol of the Northern Milky Way: A Survey for Variable Sources". *The Astrophysical Journal*, **248**, 596-605.

Gregory, P.C., and Taylor, A.R.(1986). "Radio Patrol of the Northern Milky Way. A Catalog of Sources II". *The Astronomical Journal*, **92**, 371-411.

Gull, S.F., and Daniell, G.J.(1978). "Image reconstruction from incomplete and noisy data ". *Nature*, **272**, 686-690.

Imbriale, W.A., Ingerson, P.G., and Wong, W.C.(1984). "Large Lateral Feed Displacements in a Parabolic Reflector ". *IEEE Transactions on Antennas and Propagation*, **AP-22**, 742-745.

Israel, F.P. (1976). "Aperture Synthesis Observations of Galactic H II Regions ". *Astronomy and Astrophysics*, **59**, 27-41.

Jordan, E.C. and Balmain, K.G. (1968). *Electromagnetic Waves and Radiating Systems* (2nd ed.). New Jersey: Prentice Hall.

Kay, S.M., and Marple, S.L. Jr.(1981). "Spectrum Analysis: A Modern Perspective ". *Proceedings of the IEEE*, **69**, No. 11.

Kraus, J.D.(1986). *Radio Astronomy* (2nd ed.). Ohio: Cygnus-Quasar Books.

National Radio Astronomy Observatory (1983,rev. ed). *300 foot Telescope Observer's Manual.* Green Bank, West Virginia.

Silver, S. (1944). *Microwave Antenna Theory and Design.* New York: McGraw-Hill.

Smart, W.M. (1977). *Textbook on Spherical Astronomy* (6th ed. rev. by R.M. Green). Cambridge: Cambridge University Press.

Taylor, A.R. (1982). *A Survey of the Galactic Plane for Variable Radio Emission.* Unpublished doctoral dissertation, University of British Columbia, Vancouver.

Taylor, A.R. and Gregory, P.C. (1983). "Radio Patrol of the Northern Milky Way: A Catalog of Sources. I ". *The Astronomical Journal*, **88**, 1784-1809.

Tuirri, M.E. (1964). "Radio Astronomy Receivers ". *IEEE Transactions on Antennas and Propagation*, **AP-12**, No. 7.

Appendix A - Beam Center

The beam center of the theoretical model is defined to be the point equally spaced between the maximum and minimum peak points. Given that the maximum peak position is $\vec{r_1} = (x_1, y_1, z_1)$ and the minimum peak position is $\vec{r_2} = (x_2, y_2, z_2)$, then the beam center position $\vec{r_c} = (x_c, y_c, z_c)$ is constrained by

$$\vec{r_c} \times \vec{r_1} = \vec{r_2} \times \vec{r_c} \tag{1}$$

Reduction of vector equation (1) gives

$$\frac{x_c}{x_1 + x_2} = \frac{y_c}{y_1 + y_2} = \frac{z_c}{z_1 + z_2} \tag{2}$$

Assuming that the beam center lies on a unit sphere $(x_c^2 + y_c^2 + z_c^2 = 1)$, the beam center point $\vec{r_c}$ is uniquely determined to be $x_c = \frac{x_1+x_2}{R}$, $y_c = \frac{y_1+y_2}{R}$, and $z_c = \frac{z_1+z_2}{R}$ where $R = ((x_1 + x_2)^2 + (y_1 + y_2)^2 + (z_1 + z_2)^2)^{1/2}$. Furthermore if the beam center point (θ_c, ϕ_c) is to be determined then

$$\theta_c = \arccos(z_c)$$
$$\phi_c = \arctan\left(\frac{y_c}{x_c}\right).$$

Appendix B - Oscillations

Scalar field theory was used to develop an accurate beam model for the NRAO 91 meter telescope. Physical characterstics of the NRAO 91 meter telescope and observations of point sources were used to constrain and calibrate the theoretical beam model.

During the calibration of the theoretical beam model, significant oscillations were found in the residuals between the theoretical beam model and the 0° beam rotation $60'/min$ declination driven data (called $0° - 60'/min$ driven data). Figure 28 shows a plot of the typical residuals between the theoretical beam model and the $0° - 60'/min$ driven data. The $0° - 60'/min$ residual data were analyzed and a common frequency was found. No mechanism for the oscillation was determined, but resonances in the feed support stimulated by the drive motor were suspected.

A method was derived to determine the oscillation frequency and amplitude of the $0° - 60'/min$ residuals by analyzing the results of a simulation of the oscillations in residuals. An analysis of the residuals showed that the amplitude was smallest at the beam peaks and below the 5% peak level beam, and greatest at the inflection points of the beam. In the case of the $0° - 60'/min$ driven data, there are two main lobes to the differential beam, and each beam lobe has two inflection points. Therefore the $0° - 60'/min$ driven data residuals consist of four packets of oscillations at the same frequency, with each packet centered on one inflection point of the differential beam. With this in mind, the $0° - 60'/min$ driven data residuals were divided into four residual subscans.

The endpoints of the four residual subscans were the two peak points and the four 5% level points of the $0° - 60'/min$ driven scans. Some of the residual subscans had gradient baselines. To remove the gradient baseline, the mean, the least squares fit line, and the least squares fit parabola of the residual subscan were subtracted from each residual subscan (see Figure 37). Next a baseline processed residual subscan was discarded if

one oscillation amplitude was less than three times the receiver noise of the original $0° - 60'/min$ driven scan. This reduced the number of residual subscans by half to the residual subscans from the four strongest sources.

Next the spectral density of each residual subscan was determined. It was decided that since each subscan had only approximately 17 points, a maximum entropy method should be used to determine the spectral density. The maximum entropy method (Kay *et al* 1981) requires that the model order parameter of the data to be analyzed be specified. The model order parameter, which is the order of the autoregressive process used to model the data, is 2 for the residual subscan data. Table III shows the peak frequencies of the residual subscans determined by the maximum entropy method. These results show that the average oscillation frequency in the $0° - 60'/min$ driven data is 0.65 Hz.

Table III.

Frequencies of Residual Subscans

Source Name	ν_1 Hz	ν_2 Hz	ν_3 Hz	ν_4 Hz	Average # of points
DA267	.65	.64	.64	.61	17
3C196	.59	.60	.65	.51	17
3C295	.76	.81	.70	.76	17
DA251		.60	.50	.68	18

A crude estimate of the oscillation amplitude, which is thought to be the angular distance the feed legs move, was determined from the $0° - 60'/min$ residual subscan amplitudes which are the peak residual values. The average $0° - 60'/min$ residual subscan amplitude was approximately 10% of the beam peak. The simulated residuals show that the oscillation amplitude must be at least 4.7″ for a residual subscan amplitude of 10%. Therefore the oscillation amplitude in the $0° - 60'/min$ driven data is estimated to be 4.7″ or greater.

After determination of the oscillation frequency and amplitude in the $0° - 60'/min$ driven data residuals, the same analysis was used to look for oscillations in the residuals

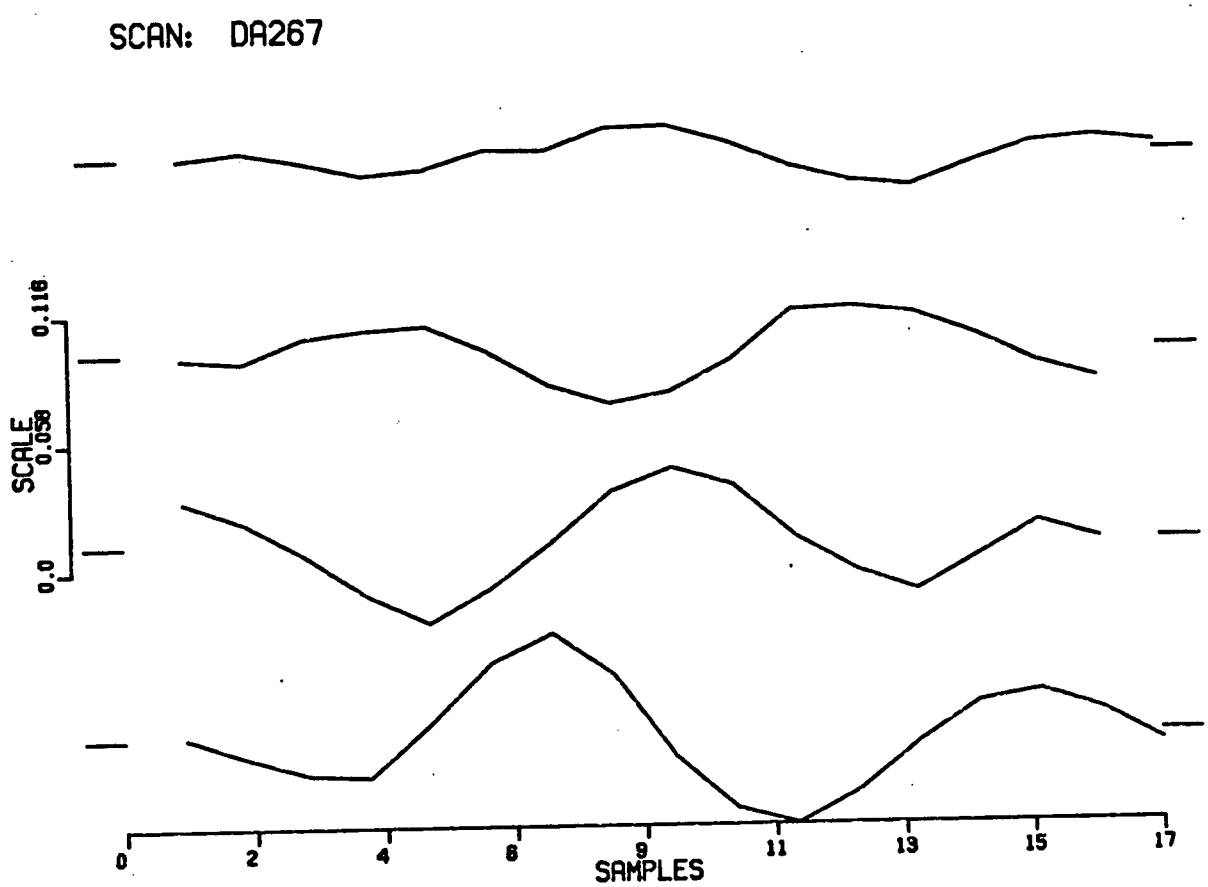

Figure 37. Plots of four baseline processed residual subscans extracted from a $0° - 60'/min$ scan through the source DA267.

of the theoretical beam model and the data driven at other declination rates. Drift scans (0'/min) were observed at both 0° and 90° rotation angles. In addition $120'/min$ declination driven scans were obtained with a beam rotation angle of 11° to the scan track. No significant oscillations were found in the residuals of the theoretical beam model and the data driven in declination at $0'/min$ and $120'/min$. The absence of the 0.65 Hz oscillations in the residuals of the beam model and the $120'/min$ data was not surprising since the telescope was driven so fast that the residual subscans were too short to measure the 0.65 Hz frequency. However, the measured telescope beamwidth was found to be larger for the $120'/min$ data than for the $0° - 60'/min$ driven data. This suggests that at the $120'/min$ drive rate the feed supports are oscillating at a higher frequency which is causing the telescope beam to appear broadened at a sampling rate of 5Hz. The $60'/min$ data provides direct evidence for a low frequency oscillation of 0.65 Hz, and the broadening of the $60'/min$ and the $120'/min$ data provides indirect evidence for high frequency oscillations. Therefore it is possible that the 0.65 Hz oscillation is one of many oscillation modes in the movement of the feeds supports.

Appendix C - Software

This appendix is a listing of the Fortran code used to generate the theoretical beam model.

Listing of ASPG:COBRA.FAST at 16:14:23 on AUG 28, 1986 for CCid=VRSS

```
      C THIS PROGRAM GENERATES A 64X64 GRIDED BEAM MODEL
      C SUITABLE FOR RUNNING ON MEMXXX. ALSO THE BEAM MAYBE
      C VIEWED ON GRIDSHOW.
      C INPUTS - UNIT 2 FEED ILLUMINATION DATA
      C OUTPUTS - UNIT 11 MODEL BEAM HEADER FILE
      C OUTPUTS - UNIT 12 MODEL BEAM GRID FILE
      C
            COMPLEX*16 EH(2,10,40)
            REAL*8 DFLOAT,H,EX
            REAL*8 RA,DE,ROT,X0,Y0,Z0,SP,CP,HB,IR,ID,DRA,DDE
            REAL*8 R0(40),KS(40),PI,BM,RT,L,X(2),Y(2)
            REAL*8 SRA,ERA,SDE,EDE,SDC,SAM,SAS,RAS,DES
            REAL*4 RB,BEAM(64,64),PK,OUT(4096),CVBEAM(64,64),G(65)
            INTEGER*4 I,J,K,N,NSTP,D,HD,WD
            COMMON /ABLOCK/ R0,KS,EH,X,Y,L,NSTP
            COMMON /BBLOCK/ X0,Y0,Z0,SP,CP,RAS
            CALL FWRITE(6,'Enter the Declination of Map: ')
            CALL FWRITE(6,'(degs,arcmins,arcsecs): ')
            CALL FREAD(5,'3(R*8): ',SDC,SAM,SAS)
            CALL FWRITE(6,'<R*8> <R*8> <R*8>: ',SDC,SAM,SAS)
            CALL FWRITE(6,'Enter the Beam rotation angle (degs): ')
            CALL FREAD(5,'R*8: ',ROT)
            CALL FWRITE(6,'<R*8>: ',ROT)
            CALL FWRITE(6,'Enter the Dec. broadening (arcsecs): ')
            CALL FWRITE(6,'(DO NOT ENTER HB EQUAL TO ZERO!): ')
            CALL FREAD(5,'R*8: ',HB)
            CALL FWRITE(6,'<R*8>: ',HB)
            CALL FWRITE(6,'Enter separtation factor: ')
            CALL FREAD(5,'R*8: ',EX)
            CALL FWRITE(6,'<R*8>: ',EX)
            CALL FWRITE(6,'Enter R.A. direction spacing(arcmins): ')
            CALL FREAD(5,'R*8: ',DRA)
            CALL FWRITE(6,'<R*8>: ',DRA)
            CALL FWRITE(6,'Enter Dec. direction spacing(arcmins): ')
            CALL FREAD(5,'R*8: ',DDE)
            CALL FWRITE(6,'<R*8>: ',DDE)
      C
      C  INITIALIZE CONSTANTS
      C
            PI=3.141592654D0
            RAS=PI
            DES=PI*(SDC+(SAM+SAS/60.D0)/60.D0)/180.D0
            RT=-PI*ROT/180.D0
            IR=DRA*PI/(10800.D0*DCOS(DES))
            ID=DDE*PI/10800.D0
            SRA=PI-32.D0*IR
            SDE=DES-33.D0*ID
            N=64
      C
      C INITIALIZE ARRAYS
      C
            CALL COEFS1
            CALL COEFS2(EX,RT,DES)
            H=HB*PI/648000.D0
            CALL CONVOL(ID,H,WD,HD,G)
      C
      C GENERATE BEAM MODEL
      C
```

```
      DO 10 J=1,64
      DE=SDE+ID*DFLOAT(J)
      DO 20 I=1,64
      RA=SRA+IR*DFLOAT(I)
      CALL CENTBM(RA,DE,BM)
      BEAM(I,J)=SNGL(BM)
   20 CONTINUE
   10 CONTINUE
C
C CONVOLVE BEAM MODEL WITH THE GAUSSIAN
C
      PK=0.
      DO 30 I=1,64
      DO 34 J=1,64
      CVBEAM(I,J)=0.
      DO 36 K=1,WD
      D=J-HD+K-1
      IF ((D.LT.1).OR.(D.GT.64)) GOTO 36
      CVBEAM(I,J)=CVBEAM(I,J)+G(K)*BEAM(I,D)
   36 CONTINUE
      RB=ABS(CVBEAM(I,J))
      IF (RB.LT.PK) GOTO 34
      PK=RB
   34 CONTINUE
   30 CONTINUE
C
C PUT NORMALIZED BEAM IN OUTPUT ARRAY
C
      DO 40 J=1,64
      DO 50 I=1,64
      K=(J-1)*64+I
      OUT(K)=CVBEAM(65-I,65-J)/PK
   50 CONTINUE
   40 CONTINUE
C
C WRITE GRIDS TYPE HEADER TO UNIT 11
C WRITE GRIDS TYPE GRID TO UNIT 12
C
      WRITE(11,100)N,N,N,SRA,SDE,IR,ID
      CALL WFILE(12,0,OUT,0,4096)
  100 FORMAT(3I6,4F10.6)
      STOP
      END
C
C THIS SUBROUTINE CALCULATES THE MODEL BEAM INTENSITY
C AT A POINT IN MODEL COORDINATES.
C
      SUBROUTINE BEAM(S,BM)
      COMPLEX*16 EH(2,10,40),I(2,2),B(2),V(2),DCONJG,DCMPLX
      REAL*8 R0(40),KS(40),X(2),Y(2),S(2),BM,DREAL,L
      INTEGER*4 J,C,M,NSTP,K
      COMMON /ABLOCK/ R0,KS,EH,X,Y,L,NSTP
C
C INITIALIZE ARRAYS
C
      DO 40 M=1,2
      DO 40 C=1,2
      I(M,C)=DCMPLX(0.D0,0.D0)
```

```
   117        40  CONTINUE
   118     C
   119     C CALCULATE INTEGRALS NUMERICALLY BY SIMPSON'S RULE.
   120     C
   121           C=2
   122           K=NSTP-1
   123           DO 20 J=1,K
   124           C=3-C
   125           CALL INTEG(S,J,B)
   126           DO 20 M=1,2
   127           I(M,C)=I(M,C)+B(M)
   128        20 CONTINUE
   129           C=NSTP
   130           CALL INTEG(S,C,B)
   131           DO 30 M=1,2
   132           V(M)=B(M)+4.D0*I(M,1)+2.D0*I(M,2)
   133        30 CONTINUE
   134     C
   135     C FIND DIFFERENTIAL BEAM INTENSITY
   136     C
   137           BM=DREAL(V(1)*DCONJG(V(1))-V(2)*DCONJG(V(2)))
   138           RETURN
   139           END
   140     C
   141     C THIS SUBROUTINE SEARCHES THE BEAM TO FIND
   142     C THE MAXIMUM AND MINIMUM PEAK POINTS.
   143     C
   144           SUBROUTINE SEARCH(SC,SS)
   145           REAL*8 SC(2),SS(2),B(5),AN(2),ST,BM,SN
   146           REAL*8 D(2,5)/0.D0,0.D0,1.D0,0.D0,0.D0,
   147          +               1.D0,-1.D0,0.D0,0.D0,-1.D0/
   148           INTEGER*4 M,I,J,JM
   149           SN=-1.D0
   150           DO 10 M=1,2
   151           SN=-SN
   152           AN(1)=SC(M)
   153           AN(2)=SS(M)
   154           CALL BEAM(AN,B(1))
   155           B(1)=SN*B(1)
   156           DO 20 I=3,9
   157           ST=(.1D0)**(I)
   158        25 JM=1
   159           BM=0.D0
   160           DO 30 J=2,5
   161           AN(1)=SC(M)+D(1,J)*ST
   162           AN(2)=SS(M)+D(2,J)*ST
   163           CALL BEAM(AN,B(J))
   164           B(J)=SN*B(J)
   165           IF ((B(J)-B(1)).LT.BM) GOTO 30
   166           JM=J
   167           BM=B(J)-B(1)
   168        30 CONTINUE
   169           IF (JM.EQ.1) GOTO 20
   170           SC(M)=SC(M)+D(1,JM)*ST
   171           SS(M)=SS(M)+D(2,JM)*ST
   172           B(1)=B(JM)
   173           GOTO 25
   174        20 CONTINUE
```

```
   175        10  CONTINUE
   176            RETURN
   177            END
   178     C
   179     C THIS SUBROUTINE CALCULATES THE COMPLEX DATA COEFICIENTS
   180     C FROM THE FEED ILLUMINATION DATA. READ FROM UNIT 2.
   181     C
   182            SUBROUTINE COEFS1
   183            COMPLEX*16 CD(2,4,40),EH(2,10,40),CDEXP,CANG,DCMPLX
   184            COMPLEX*16 CF3,CF4,CF7,CF8
   185            REAL*8 RAS,R0(40),KS(40),X(2),Y(2),X0,Y0,Z0,SP,CP
   186            REAL*8 PD(4,40),AD(2,4,40),F,A,PI,P2,P4
   187            REAL*8 SH,R,ANG,L,SPH,DPH,CPH,S2H,DARSIN,DCOS
   188            REAL*8 DSIN,DSQRT,F1,F2,F3,F4,F5,F6,F7,F8,F9,F10
   189            INTEGER*4 NSTP,J,I,M
   190            COMMON /ABLOCK/ R0,KS,EH,X,Y,L,NSTP
   191            COMMON /BBLOCK/ X0,Y0,Z0,SP,CP,RAS
   192     C
   193     C READS UNIT 2 FOR THE FEED ILLUMINATION DATA.
   194     C
   195            READ(2,150) NSTP,L
   196            READ(2,200)((PD(J,I),I=1,NSTP),J=1,4)
   197            READ(2,200)(((AD(M,J,I),I=1,NSTP),J=1,4),M=1,2)
   198       150  FORMAT(I4,F6.3)
   199       200  FORMAT(10D17.10)
   200     C
   201     C INTIALIZE CONSTANTS
   202     C
   203            F=38.735D0
   204            A=45.72D0
   205            PI=3.141592654D0
   206            P2=PI/2.D0
   207            P4=P2/2.D0
   208            SH=(A-L)/DFLOAT(NSTP)
   209     C
   210     C FILL ARRAYS TO BE USED BY SUBROUTINE INTEG.
   211     C
   212            DO 5 I=1,NSTP
   213            R=SH*DFLOAT(I)+L
   214            R0(I)=(R*R+4.D0*F*F)/(4.D0*F)
   215            DO 5 J=1,4
   216            ANG=PD(J,I)
   217            CANG=DCMPLX(0.D0,ANG)
   218            DO 5 M=1,2
   219            CD(M,J,I)=AD(M,J,I)*CDEXP(CANG)
   220          5 CONTINUE
   221            DO 50 I=1,NSTP
   222            R=SH*DFLOAT(I)+L
   223            SPH=L/R
   224            DPH=DARSIN(SPH)
   225            CPH=DSQRT((1.D0+SPH)*(1.D0-SPH))
   226            S2H=SPH*SPH
   227            F1=P2-DPH+SPH*CPH
   228            F2=P2-DPH-SPH*CPH
   229            F3=4.D0*CPH*(2.D0+S2H)/3.D0
   230            F4=8.D0/3.D0-4.D0*SPH*(1.D0-S2H/3.D0)
   231            F5=P4-DPH/2.D0+SPH*CPH*(.5D0+S2H)
   232            F6=DPH/2.D0-P4+SPH*CPH*(1.5D0+S2H)
```

```
      F7=CPH*(8.D0+S2H*(4.D0+48.D0*S2H))/15.D0
      F8=SPH*(4.D0-S2H*(20.D0/3.D0-16.D0*S2H/5.D0))-8.D0/15.D0
      F9=2.D0*SPH*S2H*CPH*(4.D0*S2H-1.D0)/3.D0
      F10=SPH*CPH*((14.D0-8.D0*S2H)*S2H/3.D0-2.D0)
      CF3=DCMPLX(0.D0,F3)
      CF4=DCMPLX(0.D0,F4)
      CF7=DCMPLX(0.D0,F7)
      CF8=DCMPLX(0.D0,F8)
      DO 52 M=1,2
      EH(M,1,I)=(CD(M,1,I)+CD(M,2,I))*F1
      EH(M,2,I)=(CD(M,3,I)+CD(M,4,I))*F2
      EH(M,3,I)=(CD(M,1,I)-CD(M,2,I))*CF3
      EH(M,4,I)=(CD(M,3,I)-CD(M,4,I))*CF4
      EH(M,5,I)=(CD(M,1,I)+CD(M,2,I))*F5
      EH(M,6,I)=(CD(M,3,I)+CD(M,4,I))*F6
      EH(M,7,I)=(CD(M,1,I)-CD(M,2,I))*CF7
      EH(M,8,I)=(CD(M,3,I)-CD(M,4,I))*CF8
      EH(M,9,I)=(CD(M,1,I)+CD(M,2,I))*F9
      EH(M,10,I)=(CD(M,3,I)+CD(M,4,I))*F10
   52 CONTINUE
   50 CONTINUE
      RETURN
      END
C
C THIS SUBROUTINE CALCULATES THE RECEIVER POSITION
C AND THEN DETERMINES THE BEAM CENTER.
C
      SUBROUTINE COEFS2(EX,RT,DES)
      COMPLEX*16 EH(2,10,40)
      REAL*8 W,L,R0(40),KS(40),X(2),Y(2),X0,Y0,Z0,SP,CP
      REAL*8 SH,DFLOAT,R,SC(2),SS(2),C(2),DSQRT,R1,RT
      REAL*8 RAS,PI,K,A,DES,EX,Z
      INTEGER*4 NSTP,I
      COMMON /ABLOCK/ R0,KS,EH,X,Y,L,NSTP
      COMMON /BBLOCK/ X0,Y0,Z0,SP,CP,RAS
C
C INITIALIZE CONSTANTS.
C
      W=0.0632D0
      Z=0.6707217897D0
      PI=3.14259265D0
      K=2.D0*PI/W
      A=45.72D0
      SH=(A-L)/DFLOAT(NSTP)
C
C CALCULATE RECEIVER POSITIONS.
C
      X(1)=-.047625D0*EX*DCOS(RT)-.4220407119D0*(Z-DES)
      Y(1)=-.047625D0*EX*DSIN(RT)-.022D0
      X(2)=+.047625D0*EX*DCOS(RT)-.4220407119D0*(Z-DES)
      Y(2)=+.047625D0*EX*DSIN(RT)-.022D0
      SP=DSIN(DES)
      CP=DCOS(DES)
      DO 10 I=1,NSTP
      R=SH*DFLOAT(I)+L
      KS(I)=K*R/R0(I)
   10 CONTINUE
      CALL INIT(SC,SS)
```

```
      CALL SEARCH(SC,SS)
      DO 20 I=1,2
      C(I)=DSQRT(1.D0-SC(I)*SC(I)-SS(I)*SS(I))
   20 CONTINUE
      R1=((SC(1)+SC(2))**2+(SS(1)+SS(2))**2+(C(1)+C(2))**2)
      R1=DSQRT(R1)
      X0=(SC(1)+SC(2))/R1
      Y0=(SS(1)+SS(2))/R1
      Z0=(C(1)+C(2))/R1
      RETURN
      END
C
C THIS SUBROUTINE CALCULATES THE BEAM IN CELESTIAL
C SPHERE COORDINATES
C
      SUBROUTINE CENTBM(RA,DE,B)
      REAL*8 RA,DE,B,ZRA,CZ,SZ,X0,Y0,Z0,SP,CP,S(2),BT
      REAL*8 DARSIN,DCOS,DSIN,RAS
      COMMON /BBLOCK/ X0,Y0,Z0,SP,CP,RAS
      ZRA=RA+DARSIN(Y0/DCOS(DE))
      CZ=Z0*DCOS(DE)*DCOS(ZRA-RA)+X0*DSIN(DE)
      CZ=CZ/((DCOS(DE)*DCOS(ZRA-RA))**2+DSIN(DE)**2)
      SZ=DSIN(DE)*CZ-X0
      SZ=SZ/(DCOS(DE)*DCOS(ZRA-RA))
      S(1)=SP*CZ-SZ*CP*DCOS(ZRA-RAS)
      S(2)=CP*DSIN(ZRA-RAS)
      CALL BEAM(S,BT)
      B=BT
      RETURN
      END
C
C THIS SUBROUTINE CALCULATES THE BEAM INTEGRAND TO BE
C USED BY BEAM. IT IS A SUM OF BESSEL FUNCTIONS.
C
      SUBROUTINE INTEG(S,N,B)
      COMPLEX*16 EH(2,10,40),B(2)
      REAL*8 JB(5),R0(40),KS(40),S(2),X(2),Y(2),U,V
      REAL*8 W,R,DSQRT,L
      INTEGER*4 NC,N,M,NSTP
      COMMON /ABLOCK/ R0,KS,EH,X,Y,L,NSTP
      DO 10 M=1,2
      U=R0(N)*S(1)+X(M)
      V=R0(N)*S(2)+Y(M)
      R=DSQRT(U*U+V*V)
      W=KS(N)*R
      CALL DBSJIN(W,5,JB,NC)
      B(M)=(EH(M,1,N)+EH(M,2,N))*JB(1)
      B(M)=B(M)+(EH(M,3,N)*V+EH(M,4,N)*U)*JB(2)/R
      B(M)=B(M)+(EH(M,5,N)+EH(M,6,N))*(U*U-V*V)*JB(3)/(R*R)
      B(M)=B(M)+(EH(M,7,N)*V*(3.D0*U*U-V*V)+
     + EH(M,8,N)*U*(U*U-3.D0*V*V))*JB(4)/(R*R*R)
      B(M)=B(M)+(EH(M,9,N)+EH(M,10,N))*
     + (V**4-6.D0*V*V*U*U+U**4)*JB(5)/(R**4)
      B(M)=KS(N)*B(M)
   10 CONTINUE
      RETURN
      END
C
```

```
      C THIS SUBROUTINE GUESSES THE VALUES FOR THE MAXIMUM
      C AND MINIMUM BEAM PEAK LOCATIONS TO BE USED BY SEARCH.
      C THE SUBROUTINE USES MODEL COORDINATES.
      C
            SUBROUTINE INIT(SC,SS)
            COMPLEX*16 EH(2,10,40)
            REAL*8 X(2),Y(2),SC(2),SS(2),R0(40),KS(40)
            REAL*8 K,KM,CDABS,L
            INTEGER*4 I,IM,NSTP,M
            COMMON /ABLOCK/ R0,KS,EH,X,Y,L,NSTP
            DO 20 M=1,2
            KM=0.D0
            DO 10 I=1,NSTP
            K=CDABS(EH(M,1,I)+EH(M,2,I))*KS(I)
            IF (K.LT.KM) GOTO 10
            IM=I
            KM=K
         10 CONTINUE
            SC(M)=-X(M)/R0(IM)
            SS(M)=-Y(M)/R0(IM)
         20 CONTINUE
            RETURN
            END
      C
      C THIS SUBROUTINE GENERATES THE ARRAY TO BE USED
      C FOR THE GAUSSIAN CONVOLUTION.
      C
            SUBROUTINE CONVOL(ID,H,WD,HD,G)
            REAL*8 ID,H
            REAL*4 G(65),A,X,M
            INTEGER*4 WD,HD,I,WE
            A=4.*ALOG(2.)/(SNGL(H)**2)
            X=SQRT(ALOG(1000.)/A)
            HD=IFIX(X/SNGL(ID))
            WD=2*HD+1
            DO 10 I=1,WD
            X=FLOAT(I-HD-1)*SNGL(ID)
            G(I)=EXP(-A*X**2)
         10 CONTINUE
            M=2.
            WE=WD-1
            DO 20 I=2,WE
            M=6.-M
            G(I)=M*G(I)
         20 CONTINUE
            RETURN
            END
      C
      C THIS SUBROUTINE WRITES DATA TO UNIT IU IN GRIDS FORMAT.
      C
            SUBROUTINE WFILE(IU,ID,X,JB,LN)
            INTEGER*2 LENGTH
            DIMENSION X(LN)
            DATA MOD/2/
            LENGTH=LN*4
            LINE=(JB/32+1)*1000
            CALL WRITE(X,LENGTH,MOD,LINE,IU,&100)
            RETURN
```

Listing of ASPG:COBRA.FAST at 16:14:23 on AUG 28, 1986 for CCid=VRSS

```
407         100  WRITE(6,101)
408         101  FORMAT('I/O error occured in WFILE')
409              STOP
410              END
```